

Dynamics of sparse Boolean networks with multi-node and self-interactions

Christian John Hurry¹, Alexander Mozeika², Alessia Annibale^{1,3}

¹Department of Mathematics, King's College London, Strand, WC2R 2LS

²School of Cancer and Pharmaceutical Sciences, King's College London, London, London, UK

³Institute for Mathematical & Molecular Biomedicine, Hodgkin Building, Guy's Campus, London, SE1 1UL

E-mail: christian.hurry@kcl.ac.uk

alexander.mozeika@kcl.ac.uk

alessia.annibale@kcl.ac.uk

Date: June 2022

Abstract. We analyse the equilibrium behaviour and non-equilibrium dynamics of sparse Boolean networks with self-interactions that evolve according to synchronous Glauber dynamics. Equilibrium analysis is achieved via a novel application of the cavity method to the temperature-dependent pseudo-Hamiltonian that characterizes the equilibrium state of systems with parallel dynamics. Similarly, the non-equilibrium dynamics can be analysed by using the dynamical version of the cavity method. It is well known, however, that when self-interactions are present, direct application of the dynamical cavity method is cumbersome, due to the presence of strong memory effects, which prevent explicit analysis of the dynamics beyond a few time steps. To overcome this difficulty, we show that it is possible to map a system of N variables to an equivalent bipartite system of $2N$ variables, for which the dynamical cavity method can be used under the usual one time approximation scheme. This substantial technical advancement allows for the study of transient and long-time behaviour of systems with self-interactions. Finally, we study the dynamics of systems with multi-node interactions, recently used to model gene regulatory networks, by mapping this to a bipartite system of Boolean variables with 2-body interactions. We show that when interactions have a degree of bidirectionality such systems are able to support a multiplicity of diverse attractors, an important requirement for a gene-regulatory network to sustain multi-cellular life.

Keywords: Dynamical cavity, replica method, random graphs, bipartite networks
Submitted to: *J. Phys. A: Math. Gen.*

1. Introduction

Sparse Boolean networks are popular models to analyse the operation of a broad range of complex systems, ranging from credit contagion [1, 2, 3] to epidemic spreading [4] and opinion dynamics [5, 6]. Originally introduced, and broadly used, to study the dynamics of gene-regulatory networks (GRNs) [7, 8], in these models each node of the network represents a gene, that is assumed to be in one of two states (expressed/not expressed), and its state is described by a Boolean variable (1 or 0). Genes are assumed to evolve synchronously in time so that all nodes of the network update together based on the state of their neighbouring nodes at the previous time step [9].

It is well known that gene expression is biologically regulated by transcription factors (TFs). These are single (or small complexes of) proteins, synthesised by genes, which can bind to certain portions of DNA, and selectively promote or inhibit the expression of genes. Recently, *bipartite* Boolean networks have been introduced to incorporate the role of TFs in the dynamics of gene expression [10, 11, 12]. In these models, genes and TFs are modelled by two sets of Boolean variables which interact with each other via directed links. A directed link from a gene to a TF indicates that the gene codes for a protein that constitutes the TF. Conversely, a directed link from a TF to a gene indicates that the TF regulates the expression of that gene. In these models, links were assumed to be sparse, directed and drawn randomly and independently from given distributions, so that links were typically unidirectional, i.e. the probability to have a bidirectional link vanished in the thermodynamic limit, where the number of nodes in the network is infinitely large, due to sparsity and directionality. Unidirectional interactions meant that genes did not contribute to the synthesis of TFs that would regulate them, a process we refer to as self-regulation. It is known that self-regulation is a common feature of GRNs, and feedback loops, where a gene is directly or indirectly involved in the regulation of its own expression, are important. It is the objective of this work to relax the assumptions made in earlier works, and allow interactions to be correlated, such that we can study the affect of self-regulation on the dynamics of GRNs.

Past models of GRNs have been shown to support only a single attractor and this was hypothesised to be due to the lack of bidirectional links in the networks that were studied [10, 11, 12]. This is consistent with recent numerical work which suggests that sparse, fully asymmetric networks tend toward supporting a single attractor as dilution is increased [13]. A study of sparsely connected, *partially* symmetric networks, to the best of our knowledge, is absent from the literature. In this work we show that partially symmetric networks can support multiple attractors, a requirement for multi-cellular life, at low, but finite, temperature. In order to do so we apply the dynamical cavity method to the study of bipartite systems, with two distinct sets of variables that evolve according to different sets of linear threshold functions. By suitable parameterisation of such systems one can study models of gene expression, with pairwise and multi-node interactions, previously studied in [10, 11, 12]. By mapping these models to suitably defined bipartite systems, we find that we can solve for the dynamics of systems with two-

body, arbitrarily asymmetric interactions, even in the presence of *self-interactions*. This represents a major technical advance, as self-interactions are well known to introduce long-time correlations which would normally make direct application of the dynamical cavity method (or equivalent methods based on generating functionals) cumbersome. By a similar mapping to bipartite networks, we are also able to investigate the dynamics of systems with multi-node (arbitrarily asymmetric) interactions, which can be regarded as Boolean equivalents of mixed p-spin models. We find that both models support, at low temperature, a multiplicity of (cyclic) attractors, as soon as a degree of bidirectionality is introduced in the links. Interestingly, multi-node interactions increase the diversity of attractors.

The remainder of this work is split into several sections. In the following section we define our model of GRNs, and include two different models of the dynamics of gene expression with pairwise and multi-node interactions, leading to linear and nonlinear dynamics, respectively. We show that both models are described by a bipartite Boolean system, and provide a general model from which the linear or nonlinear model can be recovered by suitable choice of parameters. In Sec. 3 we describe how the dynamical cavity method may be extended to bipartite spin systems, and present a closed set of equations which may be solved numerically within a one time approximation (OTA) scheme, originally developed for monopartite systems [14, 15, 16, 17]. In Sec. 4 we solve for the dynamics of the linear model of gene expression with self-interactions. Additionally, we analyse this model in equilibrium and show that is in agreement with the dynamical cavity in the steady-state. In Sec. 5 we study the nonlinear model of gene expression. We provide an assessment of the OTA scheme in the presence of nonlinear dynamics and then go on to demonstrate the existence of multiple attractors caused by bidirectional links and the impact of multi-node interactions on their diversity. In Sec. 6 we demonstrate how the dynamical cavity method may derive an efficient set of equations to solve for the dynamics of systems in the thermodynamic limit. We end with a discussion of our results, and posit further ideas for the study of multiple attractors in GRNs from a statistical mechanics perspective. Technical details are contained in the appendices.

2. Model definitions

We consider a bipartite model of gene-regulatory networks (GRNs), recently introduced in [10], which comprises N genes and $P = \alpha N$ transcription factors (TFs), with directed interactions described by two matrices, $\boldsymbol{\eta}$ and $\boldsymbol{\xi}$, giving unweighted links from genes to TFs and weighted links from TFs to genes, respectively. Entry $\eta_i^\mu \in \{0, 1\}$ denotes whether (1) or not (0) gene i contributes to the synthesis of TF μ , whereas entry $\xi_i^\mu \in \mathbb{R}$ describes the regulatory effect of TF μ on gene i , which can be excitatory ($\xi_i^\mu > 0$), inhibitory ($\xi_i^\mu < 0$) or null ($\xi_i^\mu = 0$). We will denote with $\partial_i = \{\mu : \xi_i^\mu \neq 0\}$ and $\partial_\mu = \{i : \eta_i^\mu = 1\}$ the in-neighbourhoods of gene i and TF μ , respectively, and with $d_i = |\partial_i|$ and $c_\mu = |\partial_\mu|$ their in-degrees, respectively, as sketched in figure 1.

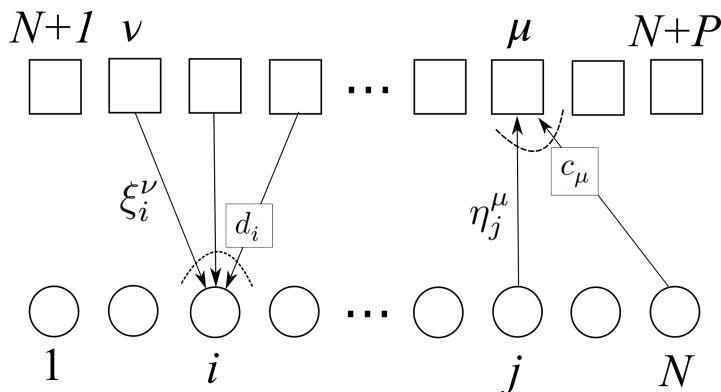


Figure 1. A sketch of the bipartite gene-TF network. Circles indicate genes, and squares indicate TFs.

Interactions are assumed sparse, as in real GRNs, i.e. the average values of the local degrees $\langle d \rangle = N^{-1} \sum_i d_i$, $\langle c \rangle = (\alpha N)^{-1} \sum_\mu c_\mu$ are $\mathcal{O}(N^0)$.

Earlier analysis of this model [10, 11, 12] regarded ξ and η as quenched random variables, drawn independently from given probability distributions $P(\xi)$ and $P(\eta)$, respectively. For this choice, the probability to observe a bidirectional link $\xi_i^\mu \eta_i^\mu \neq 0$ is $\mathcal{O}(N^{-1})$, due to the sparsity of the links, and thus vanishes in the thermodynamic limit $N \rightarrow \infty$. This assumption is however not justified by biological observations, suggesting that TFs which regulate genes contributing to their own synthesis are commonplace. In this work, we will regard ξ and η as drawn from a joint probability distribution $P(\xi, \eta) = P(\xi|\eta)P(\eta)$, such that there is a finite probability $P(\xi_i^\mu \neq 0 | \eta_i^\mu = 1) = p$ to observe a bidirectional link between a TF μ and a gene i .

Following earlier studies [10, 11, 12], we model the state of each gene, labelled by $i = 1, \dots, N$, with a Boolean variable $s_i \in \{0, 1\}$, indicating whether gene i is expressed (1) or not (0). Each TF, labelled by $\mu = N, \dots, N + P$, is associated with a variable $\tau_\mu \in [0, 1]$, which describes its concentration. Genes update their state at regular time intervals of duration Δ according to a linear threshold model,

$$s_i(t + \Delta) = \theta \left(\sum_\mu \xi_i^\mu \tau_\mu(t) + \vartheta_i - z_i(t) \right), \quad (1)$$

where $\theta(x)$ is the Heaviside step function, defined such that $\theta(x) = 1$ for $x > 0$ and $\theta(x) = 0$ for $x < 0$, ϑ_i can be thought of as a local external field or threshold and the $z_i(t)$'s are independent identically distributed zero-averaged random variables mimicking biological noise. We denote their cumulative distribution function (c.d.f.) with $\text{Prob}[z_i(t) < x] = \phi_\beta(x)$, for all i, t , where $\beta^{-1} = T$ is a parameter that characterises the noise strength. We shall assume, throughout the paper, a ‘‘thermal’’ (or Glauber) noise distribution with

$$\phi_\beta(x) = \frac{1}{2} [1 + \tanh \frac{\beta x}{2}] \quad (2)$$

Two types of dynamics for the synthesis of TFs were considered in [10, 11, 12], following different logic operations, respectively

- ‘OR’ logic

$$\tau_\mu(t) = \frac{1}{c} \sum_j \eta_j^\mu s_j(t) \quad (3)$$

where at least one gene in the in-neighbourhood of μ must be expressed for the synthesis of that TF to occur,

- ‘AND’ logic

$$\tau_\mu(t) = \prod_{j \in \partial_\mu} s_j(t) \quad (4)$$

where all genes in the in-neighbourhood of μ must be expressed for TF μ to be synthesised (in this case τ_μ takes values in $\{0, 1\}$ rather than $[0, 1]$).

If we choose that TFs evolve according to an ‘OR’ logic, upon eliminating the TFs from the description, we obtain a system of genes with their evolution given by a linear threshold model

$$s_i(t + \Delta) = \theta \left(\sum_j J_{ij} s_j(t) + \vartheta_i - z_i(t) \right) \quad (5)$$

with effective two-body interactions $J_{ij} = \sum_\mu \frac{\xi_i^\mu \eta_j^\mu}{c_\mu}$. Conversely, if TFs perform an ‘AND’ logic, the evolution of genes is given by *nonlinear* threshold dynamics

$$s_i(t + \Delta) = \theta \left(\sum_\mu \xi_i^\mu \prod_{j \in \partial_\mu} s_j(t) + \vartheta_i - z_i(t) \right), \quad (6)$$

with multi-body interactions between genes. For later convenience, it is useful to note that the ‘AND’ logic (4) can be expressed in terms of a linear threshold function with suitably chosen threshold

$$\tau_\mu(t) = \theta \left(\sum_j \eta_j^\mu s_j(t) - c_\mu + \epsilon \right) \quad (7)$$

where $0 < \epsilon \ll 1$ ensures that the argument of the step function is greater than zero when *all* of the c_μ genes contributing to TF μ are expressed and negative otherwise. Thus, an equivalent description of (6) is given by the system of equations (1) and (7). Out of mathematical convenience we will define a closely related model, where TFs are not updated instantaneously, but on the same timescale as the genes

$$\begin{aligned} s_i(t + \tilde{\Delta}) &= \theta \left(\sum_\mu \xi_i^\mu \tau_\mu(t) + \vartheta_i - z_i(t) \right) \\ \tau_\mu(t + \tilde{\Delta}) &= \theta \left(\sum_j \eta_j^\mu s_j(t) - c_\mu + \epsilon \right). \end{aligned} \quad (8)$$

Upon choosing $\tilde{\Delta} = \Delta/2$ and initial condition $\tau_\mu(0) = \theta \left(\sum_j \eta_j^\mu s_j(0) - c_\mu + \epsilon \right) \forall \mu$, the trajectory $s_i(t)$ resulting from (8) at times $t = n\Delta/2$, with $n \in \mathbb{N}$, is identical to the trajectory of (6) at times $t = n\Delta$. On the other hand, the trajectories of (8) and (6) at $t = n\Delta$ represent two independent thermal histories of the same system, as noise is drawn at each time step from the same distribution. Hence, the two systems defined in (8) and (6) are fully equivalent at integer multiples of Δ . The advantage of using (8) is that it makes the application of the dynamical cavity method straightforward (see Sec. 3).

The dynamics of GRNs evolving according to (5) has previously been studied for random interactions J_{ij} with an arbitrary degree of symmetry, in the absence of self-interactions, i.e. $J_{ii} = 0$ [18]. This corresponds, in the context of our bipartite network, to a lack of bidirectional links i.e. $\xi_i^\mu \eta_i^\mu = 0$. Similarly, the dynamics of GRNs evolving according to (6) has been studied under the assumption that $P(\boldsymbol{\xi}, \boldsymbol{\eta}) = P(\boldsymbol{\xi})P(\boldsymbol{\eta})$, such that the probability of observing a bidirectional link is zero in the limit of large system size [10, 11, 12]. It was shown in [10] that in the absence of bidirectional links this model has no multiplicity of attractors, i.e. of stable gene expression profiles, even in the absence of noise, $T = 0$. Thus, the fully asymmetric version of this model does not fulfill an important requirement for a GRN to sustain multiple cell types, as required in multi-cellular life.

In this work we solve the dynamics (5) in the presence of self-interactions, i.e. $J_{ii} \neq 0$, and the dynamics (8) in the presence of bidirectional links, i.e. $P(\xi_i^\mu \neq 0 | \eta_i^\mu = 1) = \mathcal{O}(N^0)$. Previous work has shown that dynamical analysis of (5) via generating functionals is cumbersome in the presence of self-interactions due to the strong memory effects that they produce [19], which make the complexity of the analysis exponential in the time horizon considered. We show that, while the dynamical cavity method faces a similar time-complexity barrier, when applied to the system (5) with self-interactions, it is possible, by a suitable mapping of (5) to a bipartite system $\hat{\boldsymbol{\eta}}, \hat{\boldsymbol{\xi}}$ with bidirectional links, to apply the dynamical cavity method and solve the equations explicitly under the so-called one-time approximation (OTA) scheme, that is effective in reducing the time-complexity of systems with bidirectional links [14, 15, 16, 17]. This allows us to solve the dynamics of systems with self-interactions both at short and long times, accessing in particular the non-equilibrium steady-state. To best of our knowledge, this is the first work to do so. We will define in Sec. 4 the bipartite model $\hat{\boldsymbol{\eta}}, \hat{\boldsymbol{\xi}}$ that achieves the suitable mapping, here we limit to stress that this is different from the links $\boldsymbol{\xi}, \boldsymbol{\eta}$, appearing in (1) and (3), respectively, from which the interactions $\{J_{ij}\}$ were derived. Similarly, by mapping the nonlinear threshold model (6) to the bipartite model with two-body interactions (8), we are able to solve the dynamical cavity equations in the presence of bidirectional links, under the OTA scheme, thus relaxing the assumption of fully asymmetric links used in previous work [10, 11, 12]. We will show that, upon introducing bidirectionality in the links, the nonlinear threshold model (6) is able to support a multiplicity of attractors at low noise level.

3. Dynamical cavity method for bipartite systems with parallel dynamics

As explained above, both the linear threshold model with self-interactions (5) and the nonlinear model with multi-node interactions (6) can be mapped to an equivalent bipartite system. In this section we solve the dynamics of a general bipartite system, from which either the linear or nonlinear model can be recovered by suitable choice of parameters. In this generalised model, two sets of Boolean variables, that we shall refer to as genes and TFs, update their state at regular time intervals of duration $\tilde{\Delta}$ according to the following linear threshold functions

$$s_i(t + \tilde{\Delta}) = \theta \left(\sum_{\mu} \xi_i^{\mu} \tau_{\mu}(t) + \vartheta_i - z_i(t) \right) \quad i = 1, \dots, N \quad (9)$$

$$\tau_{\mu}(t + \tilde{\Delta}) = \theta \left(\sum_j \eta_j^{\mu} s_j(t) + \vartheta_{\mu} - \hat{z}_{\mu}(t) \right) \quad \mu = N, \dots, N + P \quad (10)$$

Here, ϑ_i and ϑ_{μ} are the thresholds of gene i and TF μ , respectively, and $z_i(t)$ and $\hat{z}_{\mu}(t)$ are random i.i.d random variables with c.d.f. $\phi_{\beta}(x)$ and $\phi_{\hat{\beta}}(x)$, respectively. It is clear that (10) reduces to (8) for $\vartheta_{\mu} = -c_{\mu} + \epsilon$ and $\hat{T} = \hat{\beta}^{-1} = 0$, hence for this choice of parameters, the generalised model defined by (9) and (10) recovers model (6) with $\Delta = 2\tilde{\Delta}$ (thanks to its equivalence with (8), pointed out earlier). In Sec. 4 we will show that the system defined in (9) and (10) can also recover (5) for suitable choices of the links $\{\xi_i^{\mu}\}$ and $\{\eta_j^{\mu}\}$. For the remainder of this manuscript, we shall set $\tilde{\Delta} = 1$.

In order to solve the dynamics of the generalised model (9) and (10) we use the dynamical cavity method previously used to study systems with sparse interactions. Earlier studies have successfully applied dynamical cavity to the study of monopartite systems of Ising [14, 15, 16, 17] and Boolean [12] variables with bidirectional links, and bipartite systems of binary variables with unidirectional interactions [12]. Here we apply the method to the study of bipartite systems with (partially) bidirectional links, where each set of variables is subject to a different noise (the method would equally work for two sets of variables evolving via different dynamical rules).

We can write the probability to observe a trajectory $(\mathbf{s}^{0\dots t_m}, \boldsymbol{\tau}^{0\dots t_m})$, over time $t = 0, \dots, t_m$, for the system defined in (9) and (10), as

$$P(\mathbf{s}^{0\dots t_m}, \boldsymbol{\tau}^{0\dots t_m}) = P(\mathbf{s}^0, \boldsymbol{\tau}^0) \prod_{t=1}^{t_m} W(\mathbf{s}^t, \boldsymbol{\tau}^t | \mathbf{s}^{t-1}, \boldsymbol{\tau}^{t-1}), \quad (11)$$

where

$$W(\mathbf{s}, \boldsymbol{\tau} | \mathbf{s}', \boldsymbol{\tau}') = \prod_{i=1}^N \prod_{\mu=N+1}^{N+P} W(s_i | h_i(\boldsymbol{\tau}')) \widetilde{W}(\tau_{\mu} | h_{\mu}(\mathbf{s}'))$$

is the one-time step transition probability and, for the choice of thermal noise, (2), we

have

$$W(s_i|h_i(\boldsymbol{\tau}')) = \frac{e^{\frac{\beta}{2}(2s_i-1)h_i(\boldsymbol{\tau}')}}{2 \cosh \frac{\beta}{2}h_i(\boldsymbol{\tau}')} \quad (12)$$

$$\widetilde{W}(\tau_\mu|h_\mu(\mathbf{s}')) = \frac{e^{\frac{\beta}{2}(2\tau_\mu-1)h_\mu(\mathbf{s}')}}{2 \cosh \frac{\beta}{2}h_\mu(\mathbf{s}')} \quad (13)$$

where $h_i(\boldsymbol{\tau}) = \sum_\mu \xi_i^\mu \tau_\mu + \vartheta_i$ and $h_\mu(\mathbf{s}) = \sum_j \eta_j^\mu s_j + \vartheta_\mu$ are the local fields acting on i and μ , respectively. As the local field h_i depends only on the τ 's in the neighbourhood of i , $\boldsymbol{\tau}_{\partial_i} = \{\tau_\mu : \xi_i^\mu \neq 0\}$, we shall write $h_i(\boldsymbol{\tau}_{\partial_i})$. Similarly, we shall write $h_\mu(\mathbf{s}_{\partial_\mu})$ with $\mathbf{s}_{\partial_\mu} = \{s_j : \eta_j^\mu = 1\}$. As we detail in Appendix A, the dynamical cavity method allows us to derive an expression for the probability to observe the trajectory $s_i^{0\dots t_m}$ for the single gene i , in the cavity graph where TF ν has been removed, subject to a time dependent external field with trajectory $\zeta_i^{(\nu),1\dots t_m} = \xi_i^\nu \tau_\nu^{0\dots t_m-1}$,

$$\begin{aligned} P_i^{(\nu)}(s_i^{0\dots t_m}|\zeta_i^{(\nu),1\dots t_m}) &= P(s_i^0) \sum_{\boldsymbol{\tau}_{\partial_i \setminus \nu}^{0\dots t_m-1}} \left[\prod_{t=1}^{t_m} W(s_i^t|h_i(\boldsymbol{\tau}_{\partial_i}^{t-1})) \right] \\ &\times \prod_{\mu \in \partial_i \setminus \nu} P_\mu^{(i)}(\tau_\mu^{0\dots t_m-1}|\zeta_\mu^{(i),1\dots t_m-1}) \end{aligned} \quad (14)$$

and similarly for the trajectory of a single TF μ in the cavity graph where gene ℓ has been removed, subject to a time dependent external field $\zeta_\mu^{(\ell),1\dots t_m} = \eta_\ell^\mu s_\ell^{0\dots t_m-1}$,

$$\begin{aligned} P_\mu^{(\ell)}(\tau_\mu^{0\dots t_m}|\zeta_\mu^{(\ell),1\dots t_m}) &= P(\tau_\mu^0) \sum_{\mathbf{s}_{\partial_\mu \setminus \ell}^{0\dots t_m-1}} \left[\prod_{t=1}^{t_m} \widetilde{W}(\tau_\mu^t|h_\mu(\mathbf{s}_{\partial_\mu}^{t-1})) \right] \\ &\times \prod_{j \in \partial_\mu \setminus \ell} P_j^{(\mu)}(s_j^{0\dots t_m-1}|\zeta_j^{(\mu),1\dots t_m-1}). \end{aligned} \quad (15)$$

These expressions are exact when the bipartite network is a tree, and are expected to be a good approximation for sparse (bipartite) networks, where in the limit $N \rightarrow \infty$ the length of loops grows as $\log N$. In principle, they may be solved recursively for the probability of a trajectory up to a given time t_m . However, in expression (14) this requires a sum over $|\boldsymbol{\tau}_{\partial_i \setminus \nu}^{0\dots t_m-1}| = (2^{d_i-1})^{t_m}$ variables, which grows exponentially with time, and similarly, expression (15) requires a sum over $|\mathbf{s}_{\partial_\mu \setminus \ell}^{0\dots t_m-1}| = (2^{c_\mu-1})^{t_m}$ variables. In practice, this means that these equations can only be solved for very short times, making them unsuitable for the study of long time dynamics and stationary states. The exception is for systems with unidirectional interactions, where these equations drastically simplify (see Appendix A for details), as reported in the literature for monopartite systems [14].

When bidirectional interactions are present, an approximation scheme, known as the One Time Approximation (OTA), has been proposed to reduce the computational complexity of the dynamical cavity method [12, 14, 15, 16, 17], which factorises the

distributions of cavity trajectories into products of single time steps. Applying this approximation scheme, originally formulated for monopartite systems, to the present bipartite model, we assume

$$P_\mu^{(\ell)}(\tau_\mu^{0\dots t_m} | \zeta_\mu^{(\ell), 1\dots t_m}) = P_\mu(\tau_\mu^0) \prod_{t=1}^{t_m} P_\mu^{(\ell)}(\tau_\mu^t | \zeta_\mu^{(\ell), t}) \quad (16)$$

and

$$P_i^{(\nu)}(s_i^{0\dots t_m} | \zeta_i^{(\nu), 1\dots t_m}) = P_i(s_i^0) \prod_{t=1}^{t_m} P_i^{(\nu)}(s_i^t | \zeta_i^{(\nu), t}). \quad (17)$$

This allows us to derive an equation for the probability to observe a gene i in a given state $s_i^{t_m}$, at time t_m , in the cavity graph where TF ν has been removed, *given* the external field induced by its state at the earlier time step $\zeta_i^{(\nu), t_m} = \xi_i^\nu \tau_\nu^{t_m-1}$,

$$\begin{aligned} P_i^{(\nu)}(s_i^{t_m} | \zeta_i^{(\nu), t_m}) &= \sum_{s_i^{t_m-2}} \sum_{\tau_{\partial_i \setminus \nu}^{t_m-1}} W(s_i^{t_m} | h_i^{(\nu)}(\tau_{\partial_i}^{t_m-1}) + \zeta_i^{(\nu), t_m}) \\ &\quad \times \left[\prod_{\mu \in \partial_i \setminus \nu} P_\mu^{(i)}(\tau_\mu^{t_m-1} | \zeta_\mu^{(i), t_m-1}) \right] P_i(s_i^{t_m-2}). \end{aligned} \quad (18)$$

This depends on the probability to observe the TF μ in a given state $\tau_\mu^{t_m-1}$, at time $t_m - 1$, in the cavity graph where gene i has been removed, *given* the state of i at the earlier time step $\zeta_i^{(\nu), t_m-1} = \eta_i^\mu s_i^{t_m-2}$,

$$\begin{aligned} P_\mu^{(\ell)}(\tau_\mu^{t_m} | \zeta_\mu^{(\ell), t_m}) &= \sum_{\tau_\mu^{t_m-2}} \sum_{s_{\partial_\mu \setminus \ell}^{t_m-1}} \widetilde{W}(\tau_\mu^{t_m} | h_\mu^{(\ell)}(s_{\partial_\mu}^{t_m-1}) + \zeta_\mu^{(\ell), t_m}) \\ &\quad \times \left[\prod_{j \in \partial_\mu \setminus \ell} P_j^{(\mu)}(s_j^{t_m-1} | \zeta_j^{(\mu), t_m-1}) \right] P_\mu(\tau_\mu^{t_m-2}). \end{aligned} \quad (19)$$

As we detail in Appendix A, and as observed earlier in the literature (see [12, 14, 17]), the assumption of time factorisation is not enough to find a closed set of equations and one must make additional assumptions. In writing equations (18) and (19) we assume that the cavity distributions, with external field from the removed site, may be approximated by their non-cavity counterparts i.e

$$P_i^{(\nu)}(s_i^{T-2} | \zeta_i^{(\nu), T-2}) \approx P_i(s_i^{T-2}) \quad (20)$$

and

$$P_\mu^{(\ell)}(\tau_\mu^{T-2} | \zeta_\mu^{(\ell), T-2}) \approx P_\mu(\tau_\mu^{T-2}), \quad (21)$$

following the approach of [17]. This has recently been shown to accurately predict single-site marginals in non-equilibrium steady-states [12]. Equations (18) and (19)

then depend upon the marginal probability to observe gene i at time t_m , $P_i(s_i^{t_m})$, and TF μ at time t_m , $P_\mu(\tau_\mu^{t_m})$, which evolve according to,

$$\begin{aligned}
 P_i(s_i^{t_m}) &= \sum_{s_i^{t_m-2}} P_i(s_i^{t_m-2}) \sum_{\tau_{\partial_i}^{t_m-1}} W(s_i^{t_m} | h_i(\tau_{\partial_i}^{t_m-1})) \\
 &\times \left[\prod_{\mu \in \partial_i} P_\mu^{(i)}(\tau_\mu^{t_m-1} | \zeta_\mu^{(i), t_m-1}) \right]
 \end{aligned} \tag{22}$$

and

$$\begin{aligned}
 P_\mu(\tau_\mu^{t_m}) &= \sum_{\tau_\mu^{t_m-2}} P_\mu(\tau_\mu^{t_m-2}) \sum_{\mathbf{s}_{\partial_\mu}^{t_m-1}} \widetilde{W}(\tau_\mu^{t_m} | h_\mu(\mathbf{s}_{\partial_\mu}^{t_m-1})) \\
 &\times \left[\prod_{j \in \partial_\mu} P_j^{(\mu)}(s_j^{t_m-1} | \zeta_j^{(\mu), t_m-1}) \right].
 \end{aligned} \tag{23}$$

For a given bipartite network $(\boldsymbol{\eta}, \boldsymbol{\xi})$ and initial condition $P_i(s_i^0) \forall i$ and $P_\mu(\tau_\mu^0) \forall \mu$, one can solve these equations by simple iteration. For networks with arbitrary bidirectionality, equations (18),(19),(22) and (23) provide an efficient numerical scheme to solve for the transient and long-time dynamics of bipartite systems.

4. Linear threshold model with self-interactions

4.1. Equilibrium analysis of monopartite systems with self-interactions

In this section we analyse the equilibrium behaviour of the linear threshold model with symmetric interactions $J_{ij} = J_{ji}$, evolving via parallel dynamics (5) in the presence of self-interactions J_{ii} . It is well-known that for symmetric interactions $J_{ij} = J_{ji}$, linear threshold models evolving via parallel dynamics converge, both in the presence and the absence of self-interactions, to an equilibrium state described by the Peretto distribution, which is characterised by a temperature-dependent pseudo-Hamiltonian [20]. Equilibrium analysis of such systems has been carried out for Ising variables via transfer matrices [21, 22] and the replica method [23, 24]. An equilibrium analysis of sparse *Boolean* networks, however, is absent from the literature. Here we fill this gap by using the cavity method, originally formulated for the Gibbs-Boltzmann distribution, reached by systems evolving via sequential dynamics in the absence of self-interactions. We then use this method to study the equilibrium of the linear threshold model (5) with symmetric interactions, evolving by parallel dynamics, in the presence of self-interactions. This is described by Peretto distribution $p_{\text{eq}}(\mathbf{s}) = Z^{-1} e^{-\beta H_\beta(\mathbf{s})}$ with the *pseudo*-Hamiltonian

$$H_\beta(\mathbf{s}) = -\frac{1}{\beta} \sum_i \ln 2 \cosh \frac{\beta}{2} h_i(\mathbf{s}_{\partial_i}, s_i) - \frac{1}{2} \sum_i h_i(\mathbf{s}_{\partial_i}, s_i) - \sum_i \vartheta_i s_i \tag{24}$$

where $h_i(\mathbf{s}_{\partial_i}, s_i) = \sum_{j \in \partial_i} J_{ij} s_j + J_{ii} s_i + \vartheta_i$. The function $H_\beta(\mathbf{s})$ is not a true Hamiltonian due to its dependence on noise level, $T = \beta^{-1}$. It is helpful to introduce a fictitious

set of variables $\boldsymbol{\tau} = \{0, 1\}^N$ such that we extend our system to one of size $2N$, as it was similarly done in [23, 24] for models of Ising spins. This allows us to rewrite the equilibrium distribution as the marginal of the joint distribution of real and fictitious variables,

$$p_{\text{eq}}(\mathbf{s}) = \sum_{\boldsymbol{\tau}} p(\mathbf{s}, \boldsymbol{\tau}) \quad (25)$$

$$p(\mathbf{s}, \boldsymbol{\tau}) = \frac{1}{Z} e^{-\beta \mathcal{H}(\mathbf{s}, \boldsymbol{\tau})} \quad (26)$$

with $\mathcal{H}(\mathbf{s}, \boldsymbol{\tau}) = -\sum_{\ell, j} s_{\ell} J_{\ell j} \tau_j - \sum_{\ell} s_{\ell} J_{\ell \ell} \tau_{\ell} - \sum_{\ell} \vartheta_{\ell} (s_{\ell} + \tau_{\ell})$. In Appendix B we use the equilibrium cavity method to find a closed set of equations for single site marginals,

$$p_i(s_i, \tau_i) = \frac{1}{Z_i} e^{\beta(s_i J_{ii} \tau_i + \vartheta_i(s_i + \tau_i))} \prod_{j \in \partial_i} \sum_{s_j} \sum_{\tau_j} e^{\beta(s_i J_{ij} \tau_j + \tau_i J_{ij} s_j)} p_j^{(i)}(s_j, \tau_j) \quad (27)$$

$$p_i^{(\ell)}(s_i, \tau_i) = \frac{1}{Z_i^{(\ell)}} e^{\beta(s_i J_{ii} \tau_i + \vartheta_i(s_i + \tau_i))} \prod_{j \in \partial_i \setminus \ell} \sum_{s_j} \sum_{\tau_j} e^{\beta(s_i J_{ij} \tau_j + \tau_i J_{ij} s_j)} p_j^{(i)}(s_j, \tau_j) \quad (28)$$

which can be solved by simple iteration (see Appendix B for details). These equations are exact when the interaction matrix is a tree, and give a good approximation for sparse graphs where the length of loops grows logarithmically with the system size. From the solution of these equations we can compute the average activation probability of a site $\langle s_i \rangle = \sum_{s_i, \tau_i} s_i p_i(s_i, \tau_i)$.

To verify these equations, we now consider a system with interactions drawn according to the following probability distributions

$$P(J_{ij}) = \left(1 - \frac{c}{N}\right) \delta_{J_{ij}, 0} + \frac{c}{N} \left[\frac{1+a}{2} \delta_{J_{ij}, 1} + \frac{1-a}{2} \delta_{J_{ij}, -1} \right] \quad \forall i \neq j \quad (29)$$

$$P(J_{ii}) = (1-p) \delta_{J_{ii}, 0} + p \left[\frac{1+b}{2} \delta_{J_{ii}, 1} + \frac{1-b}{2} \delta_{J_{ii}, -1} \right] \quad \forall i \quad (30)$$

such that c and p control the density of links, and $a, b \in [-1, 1]$ control the sign of the interactions. Predictions from the cavity method are compared with results from MC simulations via

$$\langle s_i \rangle_{\text{MC}} = \frac{1}{t_l} \sum_{t=t_{\text{eq}}}^{t_l+t_{\text{eq}}} s_i^t \quad (31)$$

where t_{eq} is a large time where the system has reached equilibrium and t_l is a long time that we average the state of the site i over.

In figure 2(a), we show results for the average activation probability $a = N^{-1} \sum_i \langle s_i \rangle$, as a function of the noise level, whereas in figure 2(b), we show a scatter plot of the equilibrium activation probabilities of individual sites, at a given noise level, as predicted by the cavity method and computed from MC simulations, finding excellent agreement. It is well-known that finitely connected systems of Ising spins ($s_i \in \{-1, 1\}$) undergo a spin glass transition at low noise, where replica-symmetry is broken and

the (replica-symmetric equivalent) cavity equations are expected not to converge to the correct solution [25]. Results in figure 2(a) show, however, that in the system of sparsely connected *Boolean* variables under study, the cavity equations converge to the correct solution down to low levels of noise. Since a system of Boolean variables can be mapped to an equivalent Ising spin system by adding a quenched random external field $\vartheta_i \rightarrow \vartheta_i + \sum_j J_{ij}$ and the presence of an external field is known to change the noise level at which a finitely connected system will enter a replica-symmetry-broken phase [26, 27, 28, 29, 30], this may explain the relatively low noise level at which the cavity equations successfully converge (and replica symmetry is observed). We may expect, however, that further lowering the temperature our system may undergo ergodicity breaking, as our (non-equilibrium) analysis at zero temperature will reveal for the case of partially symmetric interactions (see Sec. 5).

In figure 3 we plot the distribution $P(\langle s_i \rangle)$ at different temperatures, as predicted by the cavity method at equilibrium, for unbiased interactions i.e. $a = 0$. In the absence of self-interactions (figures 3(a) and 3(c)), a bias in the fraction of sites that are activated in the steady state, emerges at low temperature. This is consistent with results obtained in [12] via dynamical cavity approaches (iterated until convergence), in the absence of self-interactions. Figures 3(b) and 3(d) show the distribution $P(\langle s_i \rangle)$, in the presence of self-interactions, where direct application of the dynamical cavity method would be cumbersome (see Appendix C). By choosing that all self-interactions, where present, are negative, we see that the bias in the fraction of sites which are active at low temperature is modified. For example, at relatively high temperature, we see that, in addition to the expected peak at $a_i = 1/2$ (corresponding to fluctuating variables with zero field), there is an extra peak in the presence of self-interactions, due to sites associated with the single peak having their activation probability reduced by their self-interaction.

4.2. Dynamics of monopartite spin systems with self-interactions

Previously, the dynamics of the linear threshold model (5) have been studied using the dynamical cavity method in the absence of self-interactions [12]. As we mentioned earlier, for networks with bidirectional links, the computational complexity of the cavity equations is exponential in time, due to memory effects, and the one time approximation (OTA) scheme has been proposed to reduce the computational complexity, so that the cavity equations can be solved at long and short times [14, 15, 16, 17]. However, in Appendix C we show that for systems with self-interactions the OTA scheme fails to provide a closed set of equations, and one is left with the computational complexity being exponential in time, which would prevent solving the equations at long times. To overcome this difficulty, we map our system to an equivalent bipartite system, which can be solved using the bipartite cavity equations under the OTA scheme detailed in section 3.

To map our system of N variables with interactions J_{ij} to the model defined in (9) and (10), we create an additional set of N nodes, such that the system is now of size

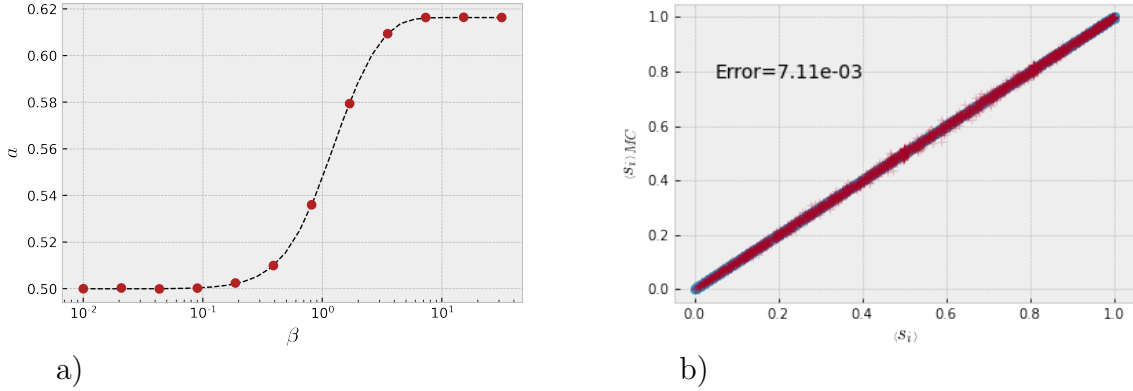


Figure 2. (a) Average activation probability of sites $a = \frac{1}{N} \sum_i \langle s_i \rangle$ against inverse noise level β . Symbols indicate the results of MC simulations, dotted line indicates solution from cavity equations (27). (b) Scatter plot of site activation probabilities $\langle s_i \rangle$ computed from static cavity method and MC simulations at noise level $\beta = 2$. Activation probability from MC simulations is computed by (31) with $t_l = 1000$ in (a) and $t_l = 5000$ in (b). In (a) and (b), the network size is $N = 5000$ with average connectivity $c = 2$, density of self-interactions $p = 0.5$ and bias $a = b = 0$. The external field is $\vartheta_i = 0 \forall i$. Annotation in (b) indicates the root mean square error.

$2N$. This means that each site in the original system is given a partner site in the new set of variables, as shown in figure 4. To achieve this we set $\eta_i^\mu = \delta_{\mu, i+N}$ in the bipartite model and $J_{ij} = \xi_i^{j+N}$. If we now set $\hat{T} = 0$ and $\vartheta_\mu = -\epsilon$ we have that (10) becomes,

$$\begin{aligned} \tau_\mu(t + \tilde{\Delta}) &= \theta(s_{\mu-N}(t) - \epsilon) \\ &= s_{\mu-N}(t) \end{aligned} \quad (32)$$

which when inserted into (9) we find,

$$s_i(t + \tilde{\Delta}) = \theta \left(\sum_{\mu=N}^{2N} \xi_i^\mu s_{\mu-N}(t - \tilde{\Delta}) + \vartheta_i - z_i(t) \right). \quad (33)$$

Hence,

$$s_i(t + \Delta) = \theta \left(\sum_{j=1}^N J_{ij} s_j(t) + \vartheta_i - z_i(t + \Delta/2) \right) \quad (34)$$

with $\Delta = 2\tilde{\Delta}$. We now see that equation (34) is of the same form as the linear threshold model with self-interactions (5). If we impose the initial conditions $\tau_{i+N}(0) = s_i(0) \forall i$, and assume that $z_i(t)$ are drawn from the same distribution (2) at each time, these two models are equivalent, up to some random noise, at every 2Δ time points. With this mapping the procedure is now as follows

- (i) Draw interaction matrix J_{ij}
- (ii) Construct bipartite system with $\xi_i^{j+N} = J_{ij}$ and $\eta_i^\mu = \delta_{\mu, i+N}$
- (iii) Solve the bipartite dynamical cavity equations up to some time t_m , with $\tilde{\Delta} = 1$

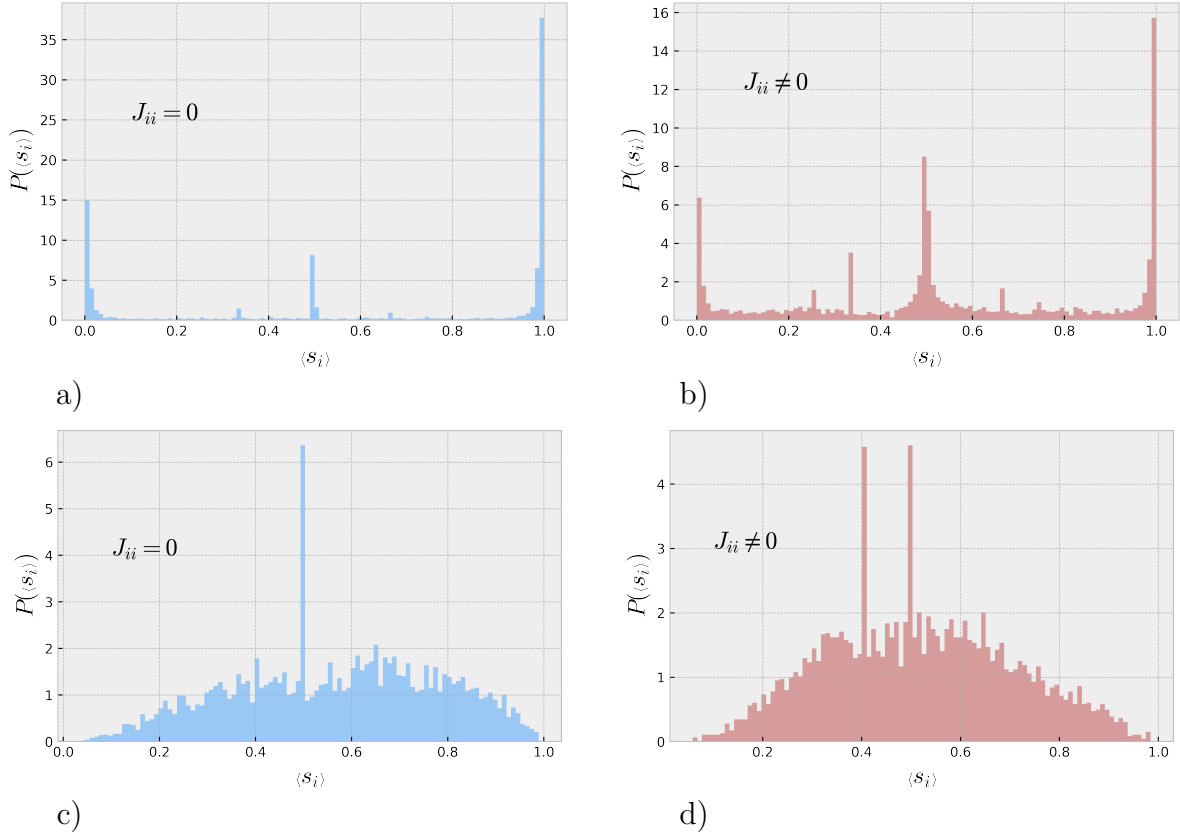


Figure 3. Probability density function for the activation probability of sites $P((s_i))$ computed from the equilibrium cavity equations. Results in each panel are for the same network of size $N = 5000$, with connectivity $c = 3$, unbiased interactions $a = 0$ and external field $\vartheta_i = 0 \forall i$. In (b) and (d), self-interactions are chosen with parameters $p = 0.5$ and $b = -1$ such that all self-interactions $J_{ii} = -1$. In (a) and (c), $J_{ii} = 0 \forall i$. In (a) and (b) inverse noise is set to $\beta = 5$, in (c) and (d) $\beta = 1$.

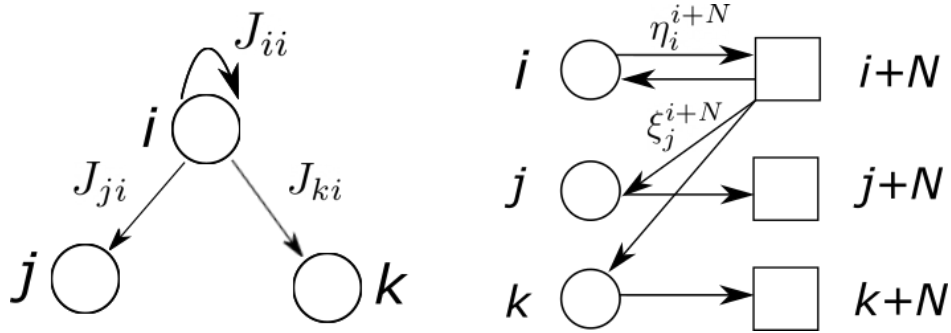


Figure 4. Sketch of how we map a monopartite system with self-interactions (left) to an equivalent bipartite spin system (right). In this mapping we have that the interaction site i has on site j is given by $J_{ji} = \xi_j^{i+N}$, and we have $\eta_i^i = \delta_{i,i+N}$.

(iv) Compare with MC simulations of the monopartite system (5) at $t = 0, 2, 4, \dots, t_m$. We follow this procedure and compute the activation probability of each site obtained via dynamical cavity applied to the bipartite system and via MC simulations of the

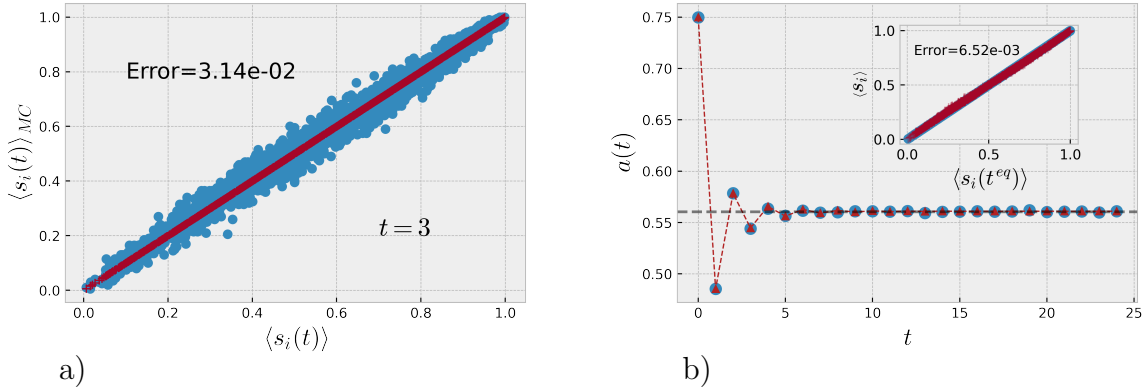


Figure 5. (a) Scatter plot of site activation probabilities $\langle s_i(t) \rangle$ computed via dynamical cavity and from MC simulations (average over 200 runs with different initial conditions drawn from the same distribution). (b) Site average of activation probabilities against time. Circles indicate MC simulations, triangles, connected by red dashed line for visual aid, indicate the solution of the bipartite dynamical cavity equations, (22) and (23). Dashed horizontal line indicates the solution for average activation found from the cavity equations at equilibrium (27). Inset of (b) shows scatter plot of activation probability of each spin computed from equilibrium cavity and dynamical cavity method in the steady state. Annotation indicates the root mean square error. In (a) and (b), network size is $N = 2500$, connectivity $c = 2$, density of self-interactions $p = 0.25$, bias $a = b = 0$, external field $\vartheta_i = 0 \forall i$, noise level $\beta = 1.5$, and initial conditions $P(s_i^0) = P(\tau_\mu^0) = 0.75$.

equivalent monopartite system. Figure 5(a) shows results for the transient behaviour where the dynamical cavity method accurately predicts the activation probability of each site. Figure 5(b) shows the full time dependence of the average activation probability and agreement is excellent both during transient and in the steady state. Additionally, the inset of figure 5(b) shows that the stationary state reached by the bipartite dynamical cavity method is in excellent agreement with the equilibrium state predicted by the static cavity equations. Therefore, by mapping a monopartite system with self-interactions to an equivalent bipartite system, we can now study their transient and long-time dynamics.

5. Nonlinear model with correlated, multi-node interactions

5.1. Dynamical analysis of systems with multi-node interactions

Previously, the dynamics of the nonlinear model (6) has been studied under the assumption that interactions are uncorrelated, $P(\boldsymbol{\xi}, \boldsymbol{\eta}) = P(\boldsymbol{\xi})P(\boldsymbol{\eta})$, and in the absence of noise in TF synthesis, $\hat{T} = 0$ [10, 12]. Here we solve the dynamics of the system defined in (8), from which the dynamics of (6) can be recovered, with arbitrary noise \hat{T} in TF synthesis and correlated interactions $P(\boldsymbol{\xi}, \boldsymbol{\eta}) = P(\boldsymbol{\xi}|\boldsymbol{\eta})P(\boldsymbol{\eta})$. We will assume

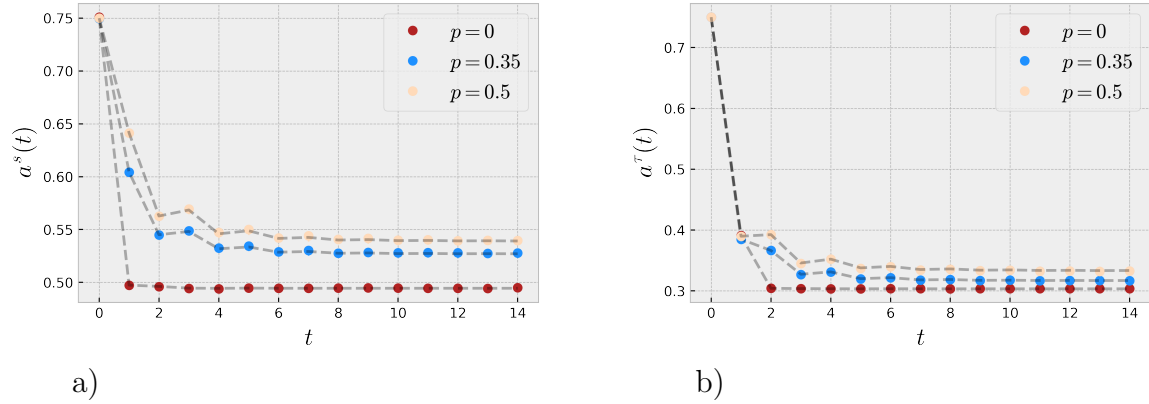


Figure 6. Average activation of (a) genes $a^s(t) = N^{-1} \sum_i \langle s_i(t) \rangle$ and (b) TFs, $a^\tau(t) = (\alpha N)^{-1} \sum_\mu \langle \tau_\mu(t) \rangle$ against time. Markers indicate MC simulations on networks with size $N = 2500$ averaged over 100 runs with initial conditions drawn from $P(s_i^0) = P(\tau_\mu^0) = 0.75 \forall i, \mu$. Noise level is $\beta = \hat{\beta} = 10$, network parameters are $c = 1, d = 2, a = 0, b = 1$. Results shown for different densities of self-interactions, p , as indicated in the legend.

$P(\boldsymbol{\eta}) = \prod_{i,\mu} P(\eta_i^\mu)$ with

$$P(\eta_i^\mu) = \left(1 - \frac{c}{N}\right) \delta_{\eta_i^\mu, 0} + \frac{c}{N} \delta_{\eta_i^\mu, 1} \quad (35)$$

and $P(\boldsymbol{\xi}|\boldsymbol{\eta}) = \prod_{i,\mu} P(\xi_i^\mu|\eta_i^\mu)$, with the choice

$$P(\xi_i^\mu|\eta_i^\mu = 0) = \left(1 - \frac{d}{N}\right) \delta_{\xi_i^\mu, 0} + \frac{d}{N} \left[\frac{1+a}{2} \delta_{\xi_i^\mu, \frac{1}{d}} + \frac{1-a}{2} \delta_{\xi_i^\mu, -\frac{1}{d}} \right] \quad (36)$$

$$P(\xi_i^\mu|\eta_i^\mu = 1) = (1-p) \delta_{\xi_i^\mu, 0} + p \left[\frac{1+b}{2} \delta_{\xi_i^\mu, 1} + \frac{1-b}{2} \delta_{\xi_i^\mu, -1} \right] \quad (37)$$

such that c is the average in-degree of a TF and $d + pc$ is the average out-degree of a TF, d being the average number of unidirectional links stemming from a TF and pc the average number of bidirectional links stemming from (and pointing to) a TF. In particular, $p \in [0, 1]$ controls the density of bidirectional links, such that the network is unidirectional when $p = 0$, and when $p = 1$ any gene that contributes to the synthesis of a TF will be regulated by that TF, in which case the number of bidirectional links in the network is maximal and equal to $\alpha c N$. We note that when $p = 1$ the network is not fully bidirectional as $\eta_i^\mu = 0$ does not imply $\xi_i^\mu = 0$ and there are still $\alpha d N$ unidirectional links from TFs to genes. The bias in positive and negative regulatory couplings is controlled through the parameters $a, b \in [-1, 1]$ such that all regulatory effects are excitatory ($\xi > 0$) if $a, b = 1$ and all are inhibitory ($\xi < 0$) if $a, b = -1$.

To assess the accuracy of the dynamical cavity method, we compute the time-dependent average activation probability of genes and TFs, given by $\langle s_i(t) \rangle = \sum_{s_i} s_i^t P_i(s_i^t)$ and $\langle \tau_\mu(t) \rangle = \sum_{\tau_\mu} \tau_\mu^t P_\mu(\tau_\mu^t)$, respectively. To compute this from MC simulations, we run many thermal realisations of a trajectory and take the average

over these thermal realisations,

$$\langle s_i(t) \rangle_{\text{MC}} = \frac{1}{n} \sum_{\rho=1}^n s_i^{t,\rho} \quad (38)$$

$$\langle \tau_\mu(t) \rangle_{\text{MC}} = \frac{1}{n} \sum_{\rho=1}^n \tau_\mu^{t,\rho} \quad (39)$$

where n is the number of thermal realisations of the trajectory we average over, and $s_i^{t,\rho}, \tau_\mu^{t,\rho}$ denote the states of gene i and TF μ at time t in the ρ^{th} realisation of the trajectory, respectively. In figure 6 we show the average activation probability of genes and TFs against time, and show that there is good agreement between the dynamical cavity method and MC simulations at all times, for different densities of bidirectional links and relatively low temperature. Additionally, the stationary values of the activation probabilities of individual sites are plotted in figure 7 for the same temperature and are found in good agreement with MC simulations.

It is well known that the error in the predictions from the dynamical cavity method under the OTA scheme increases as the noise level is decreased. Previous work has demonstrated this looking at the error of macroscopic quantities in Ising spin models [15, 16] whereas for Boolean systems with pairwise interactions, such as the linear threshold model (5), predictions within a OTA scheme were found to remain accurate for microscopic quantities, even at relatively low temperatures. Here, we assess the accuracy of the OTA scheme in predicting microscopic quantities in Boolean systems with multi-node interactions, like the non-linear threshold model defined in (6), and we find that the accuracy of OTA decreases when the temperature is lowered, similarly to what was observed in Ising spin models. In figure 8(a) we show the mean square error in activation probabilities, $\delta(t) = N^{-1} \sum_i (\langle s_i(t) \rangle - \langle s_i(t) \rangle_{\text{MC}})^2$, at zero noise. For networks with an absence of bidirectional links, the OTA scheme is in perfect agreement with the MC simulations at long times, when the system has reached equilibrium. The accuracy of the OTA scheme at zero noise, however, decreases as the density of bidirectional links increases. There are two potential sources of error. Firstly, the OTA scheme is based on two explicit assumptions, i.e. the Markovian factorization of cavity trajectories, (16) and (17), and the closure assumption, (20) and (21), which may break down at lower temperature due to stronger memory effects. Secondly, the dynamical cavity method implicitly assumes that there is no ergodicity breaking. Practically, the assumption that the system is ergodic in the cavity approach means that when we provide the dynamical cavity method with the initial conditions $P_0(\mathbf{s}^0) = \prod_i P_0(s_i^0)$ and $P_0(\boldsymbol{\tau}^0) = \prod_\mu P_0(\tau_\mu^0)$, it is implied that each configuration drawn from this distribution belongs to the same *ergodic sector*, and will hence reach the same attractor, which is untrue when ergodicity is broken. To deduce whether the loss of accuracy at zero temperature is due to the assumptions made in the OTA scheme, or by ergodicity breaking, we provide the dynamical cavity equations with a *specific configuration* ($\mathbf{s}^0, \boldsymbol{\tau}^0$) as the initial condition, and then run zero temperature dynamics. In figure 8(b) we show that by initializing

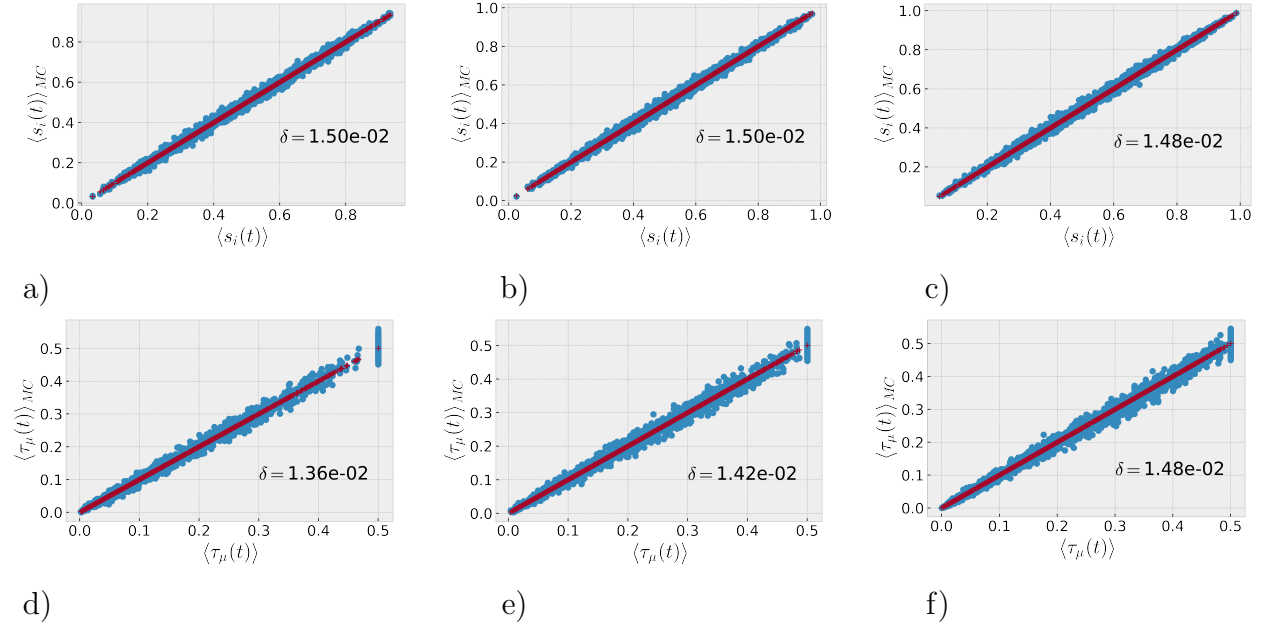


Figure 7. Scatter plot of the activation probability of genes $\langle s_i(t) \rangle$ (a)-(c) and TFs $\langle \tau_\mu(t) \rangle$ (d)-(f) from dynamical cavity method and MC simulations. MC simulations are averaged over 1000 thermal histories. Here we show the system at time $t = 15$ where the system has reached its steady-state. Parameters are: $N = 2500$, $c = 1$, $d = 2$, $a = 0$, $b = 1$, $\beta = \hat{\beta} = 10$. The root mean square error δ for each plot is annotated. Columns correspond to different densities of bidirectional links, from left to right $p = 0, 0.35, 0.5$.

dynamical cavity in the same configuration (and thus in the same ergodic sector) as MC simulations, the OTA scheme predicts the trajectory without error. This suggests that the loss of accuracy observed in figure 8(a) is due to ergodicity breaking.

5.2. Multiple attractors induced by self-regulation

The evidence of ergodicity breaking suggests that our system supports multiple attractors. To confirm this we show in figures 9(a) and 9(c) the dynamics of genes and TFs starting from two different initial conditions for the same network. In the network we consider, a TF has an excitatory effect on every gene that is required for its own synthesis, $p = 1$ and $b = 1$, such that this network has a high density of bidirectional links. We again initialise the dynamical cavity method with the same initial configuration as the MC simulations, such that there is zero error in the dynamical cavity predictions. We see that the dynamics of the same network, starting from two different initial configurations, converges to two different 2-cycles, which shows that, at least at zero temperature, our model supports multiple attractors.

To better assess the type of attractors these systems exhibit, we look at the self-

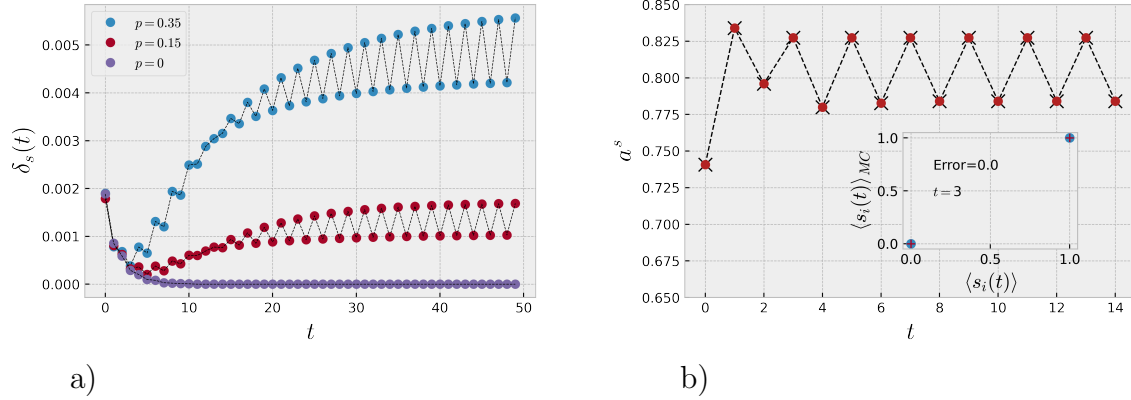


Figure 8. (a) Mean square error $\delta_s(t)$ between MC simulations (averages over 100 runs) and dynamical cavity, for the activation probabilities of genes, against time. Network size is $N = 2500$, connectivities are $c = 1$, $d = 2$, bias are $a = 0$, $b = 1$, and initial conditions are set to $P(s_i^0) = P(\tau_\mu^0) = 0.75$. Results shown for different densities of self-interactions, p , as indicated in the legend. (b) Average activation probability of genes $a^s(t) = N^{-1} \sum_i \langle s_i(t) \rangle$ against time, computed by dynamical cavity (crosses) and MC simulations (circles). The dynamical cavity method is initialised with $P_i(s_i^0) = \delta_{s_i^0, s_i^{MC(0)}}$ and $P_\mu(\tau_\mu^0) = \delta_{\tau_\mu^0, \tau_\mu^{MC(0)}}$. Network parameters are: $N = 1500$, $c = 1$, $d = 3$, $a = -1.5$, $b = 1$. Inset shows scatter plot of site activation probabilities of genes $\langle s_i(t) \rangle$, at time $t = 3$, computed by dynamical cavity and MC simulations. Annotation indicates root mean square error. In (a) and (b) external fields are set to $\vartheta_i = \epsilon$ and $\vartheta_\mu = -c_\mu + \epsilon$, with $\epsilon = 10^{-4}$, and the noise level is $\beta = \hat{\beta} = \infty$.

overlap, which we define as,

$$\Gamma^s(t, t') = \frac{1}{N} \sum_i (s_i^t - s_i^{t'})^2 \quad (40)$$

$$\Gamma^\tau(t, t') = \frac{1}{N} \sum_\mu (\tau_\mu^t - \tau_\mu^{t'})^2. \quad (41)$$

By running MC simulations at zero temperature for some long time t_w , and computing the self-overlap $\Gamma^s(t, t_w)$, with all other times $t \leq t_w$, we find, as shown in figures 9(b) and 9(d), that for systems with all positive self-regulatory effects the system will exhibit a 2-cycle, but the same network where the self-regulatory effects are negative will exhibit a 4-cycle. We find these results consistent for different realisations of the network, and for networks with different values of TF in-degree, $d + pc$. This suggests that the type of attractor that the dynamics converges to is determined by the type of self-regulatory effects present, alone.

To elucidate the effect that the density of bidirectional links has on the attractors of our model, we study a dynamical variant of the overlap distribution. We exploit the fact that we are at zero temperature to run MC simulations until the system reaches its attractor, store them, and compare the attractors that are reached from different initial conditions. At zero temperature, the system is expected to reach a limit cycle, and so we compute the overlap between each point of the limit-cycles reached from two random

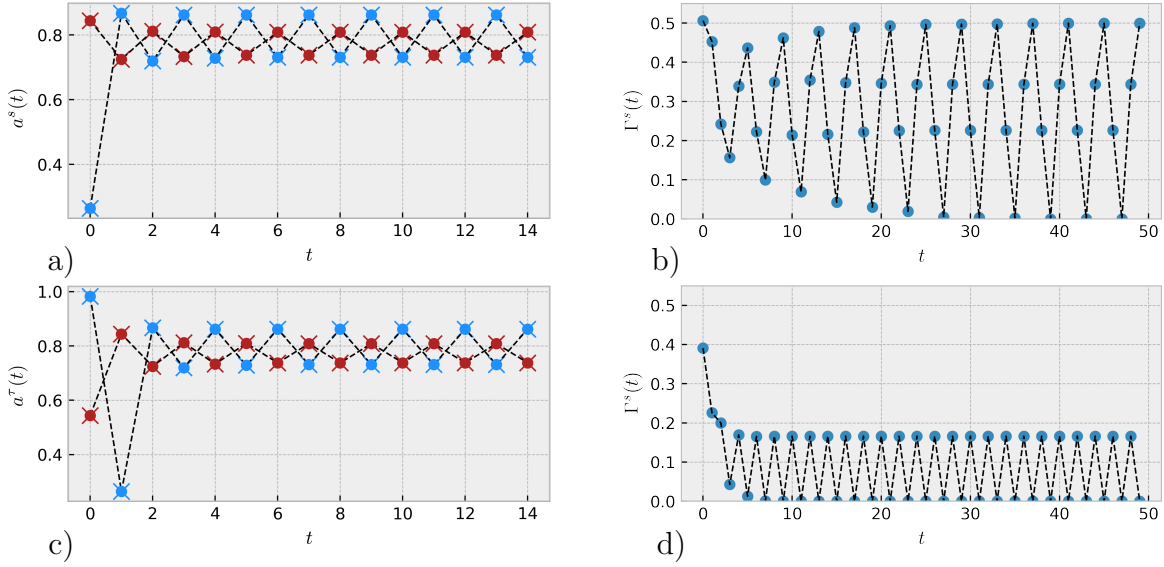


Figure 9. (a) and (c): Average activation of genes (a) and TFs (c) with system size $N = 1500$, $c = 1$, $d = 3$, $a = -1.5$, $b = 1$ (i.e. all self-interactions are positive) and $\beta = \hat{\beta} = \infty$. Results for two different initial conditions are shown. Circles indicate MC simulations, crosses indicate dynamical cavity. The dynamical cavity method is initialised with $P_i(s_i^0) = \delta_{s_i^0, s_i^{MC}(0)}$ and $P_\mu(\tau_\mu^0) = \delta_{\tau_\mu^0, \tau_\mu^{MC}(0)}$. (b) and (d): Self-overlap $\Gamma^s(t, T)$ against time t for genes. Results are computed from MC simulations with $N = 2500$, $c = 1$, $d = 15$, $a = 0$, for cases where (b) all self-interactions are inhibitory (i.e. $b = -1$) or (d) excitatory (i.e. $b = 1$). Similar plot can be obtained for the self-overlaps of the TFs, $\Gamma^\tau(t, T)$ but are not shown here.

initial conditions. The overlap for two replicas, \mathbf{s}^ρ and \mathbf{s}^ν , of the system starting from different random initial conditions is defined as

$$q_{\rho\nu}^s = \frac{1}{N} \sum_i \sum_{n=1}^p (2s_i^{n,\rho} - 1) (2s_i^{n,\nu} - 1) \quad (42)$$

where $s_i^{n,\rho}$ is the state of site i at the n^{th} point in the limit cycle in replica ρ . We can similarly define the overlap for the TFs,

$$q_{\rho\nu}^\tau = \frac{1}{N} \sum_\mu \sum_{n=1}^p (2\tau_\mu^{n,\rho} - 1) (2\tau_\mu^{n,\nu} - 1) \quad (43)$$

The overlap takes values in $q \in [-1, 1]$ such that $q = 1$ if the configurations are identical, and $q = -1$ if they are oppositely aligned i.e. $s_i^\rho = 1 - s_i^\nu \forall i$. The above definition of the overlap is, however, dependent on the ordering of the points in the cycle. For example, it may be that two initial conditions lead to the same attractor, but enter the attractor at different points in the cycle, and so lead to an overlap $q \neq 1$. For this reason we compute the overlap between the attractors for different permutations of the points in the cycle and take the *maximum* value to be the true value of the overlap. By drawing many pairs of initial conditions and computing the overlap between the attractors according to the above, we compute the overlap distribution. Figure 10 shows that as the density of

bidirectional links decreases, the width of the overlap distribution decreases and moves towards an overlap of $q_{12}^s, q_{12}^t = 1$, suggesting that the attractors become more similar as bidirectional links are removed, and that systems without bidirectional links will have just one attractor. Additionally, the external field acting on the TFs is shown to have a significant effect. When $\vartheta_\mu = -c_\mu + \epsilon$, such that TFs operate with AND logic, we see the existence of multiple attractors, with relatively low overlap (figures 10(a) and 10(d)). Conversely, for systems with external field $\vartheta_\mu = -\epsilon$, such that TFs operate with OR logic, we see that while these networks do support multiple attractors, the overlap is high, hence the attractors are very similar (figures 10(c) and 10(f)). Interpolating between these extreme cases, we set $\vartheta_\mu = -1 - \epsilon$, to add a little cooperativity to the OR logic, such that a TF requires at least two neighbouring genes to be active in order to be synthesised. In this case, we also see high overlap, even for systems with high densities of bidirectional links (figures 10(b) and 10(e)).

Our work demonstrates the existence of multiple attractors in sparse, partially bidirectional networks. Previous analytical work has focused on the fully connected and fully asymmetric cases [31, 32, 33]. More recently, numerical studies in small sparse networks showed that the number of attractors decreases to one as the dilution of the network is increased [13]. Our results show that the presence of bidirectional links is crucial to have a multiplicity of attractors in sparse networks and that increasing the fraction of bidirectional interactions decreases the overlap between the attractors of the system. To the best of our knowledge, our work is the first to demonstrate that the existence of multiple attractors in sparse networks is conditional on the interactions being at least partially bidirectional.

Additionally, we have seen that the overlap is lower in the nonlinear model, where TFs evolve according to AND logic, than in the linear model, where TFs evolve according to OR logic, suggesting that cooperativity in gene regulation promotes diversification of attractors. Our nonlinear model can be regarded as the Boolean equivalent of a mixed p-spin model, where the state of each site depends on a varying number of sites. The regular p-spin model has been shown in equilibrium to exhibit a replica symmetry breaking phase at low noise levels, where ergodicity is broken and multiple attractors are to be expected [34, 35, 36]. Our numerical results show that ergodicity is also broken in our mixed p-Boolean model with asymmetric interactions, at low levels of noise, where the system exhibits a multiplicity of *cyclic* attractors. Interestingly, the overlap distribution is reminiscent of the one observed in equilibrium spin models exhibiting one step of replica symmetry breaking. It can be shown that the width of the distributions in figure 10 decreases with system size as $N^{-\frac{1}{2}}$, suggesting that this is a finite size effect and that for networks of infinite size these distributions are delta-peaked at a single value.

While we have shown the existence of multiple attractors in the absence of noise, we expect that as noise is increased, the system will become ergodic, and the dynamics will converge to a single attractor. We can, however, show in figure 11 that if TFs evolve without noise, but genes evolve with low but finite noise, the system still

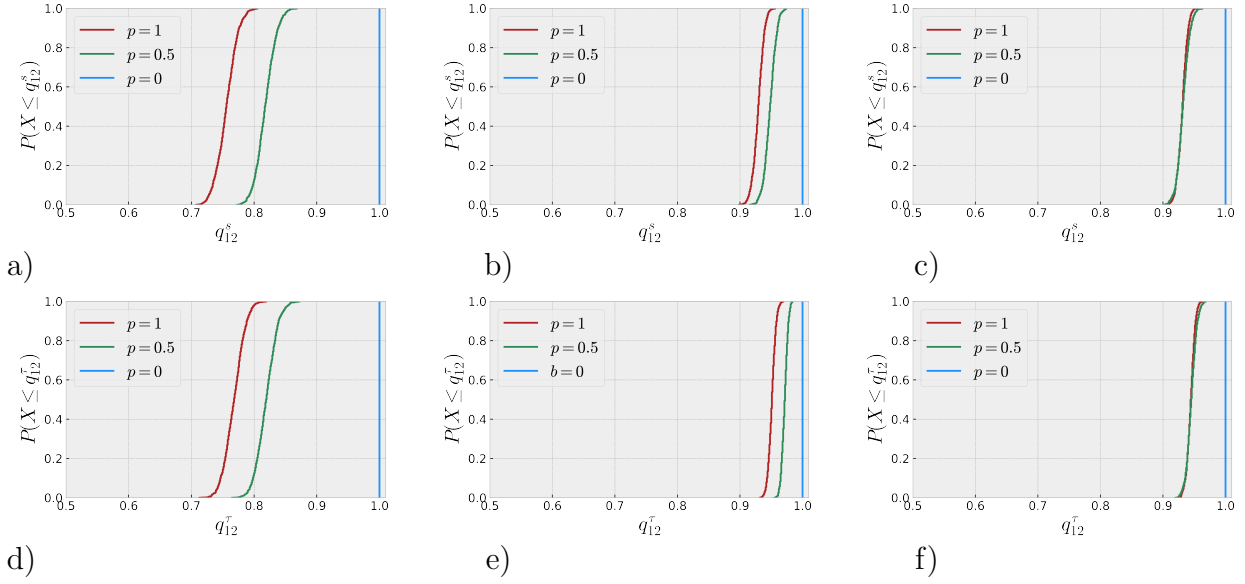


Figure 10. Distribution of overlap of attractors starting from two different initial conditions for genes $P(q_{12}^s)$ (a)-(c) and TFs $P(q_{12}^{\tau})$ (d)-(f). Network parameters are: $N = 1000$, $c = 1$, $d = 3$, $a = 0$, $b = 1$. Distributions are formed by comparing the attractors reached by 1000 random pairs of initial conditions. Results shown for different levels of bidirectional links indicated by legend. Noise level is $\beta = \hat{\beta} = \infty$. Columns, from left to right, indicate cases where $\vartheta_{\mu} = -c_{\mu} + \epsilon$, $\vartheta_{\mu} = -1 - \epsilon$ and $\vartheta_{\mu} = -\epsilon$ with $\epsilon = 10^{-4}$. We also have $\vartheta_i = \epsilon$.

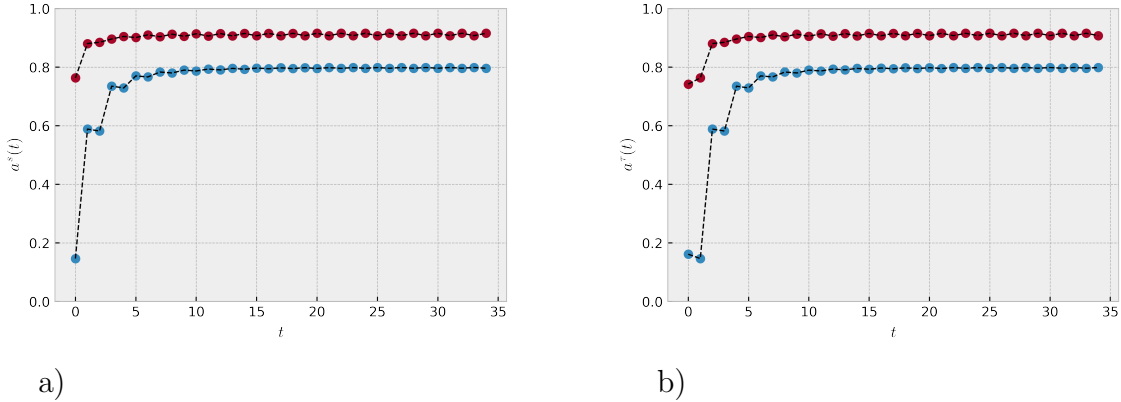


Figure 11. Average activation of (a) genes $a^s(t) = N^{-1} \sum_i \langle s_i(t) \rangle$ and (b) TFs $a^{\tau}(t) = (\alpha N)^{-1} \sum_{\mu} \langle \tau_{\mu}(t) \rangle$ against time. Symbols indicate result of MC simulations averaged over 100 thermal histories. Network parameters are: $N = 1500$, $c = 1$, $d = 10$, $p = 1$, $a = 0$ and $b = 1$. Noise level for TFs $\hat{\beta} = \infty$ and for genes $\beta = 100$.

exhibits multiple attractors. Here, we have used a network with higher degree than in figures 9(a) and 9(c) and see that there is a bigger difference in the average activation, suggesting that as the connectivity of the network is increased, the attractors become more dissimilar. Finally, we observe that any low but finite noise in the TFs dynamics leads to a single attractor, even when gene dynamics is noiseless.

6. OTA in the thermodynamic limit

In earlier sections we have derived expressions for activation probabilities of individual nodes in single graph instances. We can use these results to obtain expressions for typical (or average) activation probabilities by averaging over sites. For large networks, these expressions will depend on the distribution $P(\mathbf{J})$ (or $P(\boldsymbol{\eta}, \boldsymbol{\xi})$) of the disorder and not on its realization \mathbf{J} (or $\boldsymbol{\eta}, \boldsymbol{\xi}$), hence they give information on typical trajectories in the graph ensemble. Similar expressions can also be derived via generating functional analysis (GFA) [37, 38], however, no equivalent of the OTA scheme has been formulated within GFA, hence the resulting equations exhibit the aforementioned exponential time complexity. Taking averages of the dynamical cavity equations after application of the OTA scheme allows us to obtain equations for typical activation probabilities which do not exhibit such complexity and can therefore be solved explicitly at short and long times.

To demonstrate this we consider the linear threshold model (5) in the absence of self-interactions, such that $J_{ii} = 0$. In this case the probability of a site to have activation s_i^t at some time t , under the OTA scheme, is given by,

$$P_i(s_i^t) = \sum_{s_i^{t-2}} P_i(s_i^{t-2}) \sum_{\mathbf{s}_{\partial_i}^{t-1}} W(s_i^t | h_i(\mathbf{s}_{\partial_i}^{t-1})) \left[\prod_{j \in \partial_i} P_j^{(i)}(s_j^{t-1} | \zeta_j^{(i), t-1}) \right], \quad (44)$$

and the probability of a site to have activation s_i^t at time t , in the cavity graph where site ℓ is removed, subject to some external field $\zeta_i^{(\ell), t} = J_{i\ell} s_\ell^{t-1}$, is given by

$$P_i^{(\ell)}(s_i^t | \zeta_i^{(\ell), t}) = \sum_{s_i^{t-2}} P_i(s_i^{t-2}) \sum_{\mathbf{s}_{\partial_i \setminus \ell}^{t-1}} W(s_i^t | h_i(\mathbf{s}_{\partial_i}^{t-1})) \left[\prod_{j \in \partial_i \setminus \ell} P_j^{(i)}(s_j^{t-1} | \zeta_j^{(i), t-1}) \right] \quad (45)$$

as shown in [17]. From this we can define the distribution of site marginals as,

$$\pi(\{P_t\}) = \frac{1}{N} \sum_i \prod_{s^t} \delta(P_t(s^t) - P_i(s^t)). \quad (46)$$

In Appendix D we show that in the limit $N \rightarrow \infty$ the distribution of site marginals is found from the following closed set of equations,

$$\begin{aligned} \pi(\{P_t\}) &= \sum_k P(k) \int \left[\prod_{j=1}^k dJ_j d\hat{J}_j \{d\hat{P}_j\} P(J_j) P(\hat{J}_j | J_j) \right] \int \{dP_{t-2}\} \\ &\times \pi_{t-2} \left[\{P_{t-2}\} | k, \mathbf{J}, \hat{\mathbf{J}} \right] \prod_{s^t} \delta \left(P_t(s^t) - \phi(k, \{P_{t-2}\}, \mathbf{J}, \hat{\mathbf{J}}, \{\hat{\mathbf{P}}\}) \right) \\ &\times \prod_{j=1}^k \hat{\pi}_{t-1} \left[\{\hat{P}_j\} | \hat{J}_j s^{t-2} \right] \end{aligned} \quad (47)$$

with

$$\phi(k, \{\mathbf{P}_{t-2}\}, \mathbf{J}, \hat{\mathbf{J}}, \{\hat{\mathbf{P}}\}) = \sum_{s^{t-2}} \mathbf{P}_{t-2}(s^{t-2}) \sum_{s_1^{t-1}, \dots, s_k^{t-1}} W(s^t | \sum_{j=1}^k J_j s_j^{t-1}) \prod_{j=1}^k \hat{\mathbf{P}}_j(s_j^{t-1}) \quad (48)$$

and

$$\begin{aligned} \hat{\pi}_t(\{\mathbf{P}_t\}|x) &= \sum_k \frac{kP(k)}{\langle k \rangle} \int \left[\prod_{j=1}^{k-1} dJ_j d\hat{J}_j \{d\hat{\mathbf{P}}_j\} P(J_j) P(\hat{J}_j | J_j) \right] \int \{d\mathbf{P}_{t-2}\} \\ &\times \pi_{t-2} \left[\{\mathbf{P}_{t-2}\} | k, \mathbf{J}, \hat{\mathbf{J}} \right] \prod_{s^t} \delta \left(\mathbf{P}_t(s^t) - \tilde{\phi}(k, \{\mathbf{P}_{t-2}\}, \mathbf{J}, \hat{\mathbf{J}}, \{\hat{\mathbf{P}}\}, x) \right) \\ &\times \prod_{j=1}^{k-1} \hat{\pi}_{t-1} \left[\{\hat{\mathbf{P}}_j\} | \hat{J}_j s^{t-2} \right] \end{aligned} \quad (49)$$

where we define,

$$\begin{aligned} \tilde{\phi}(k, \{\mathbf{P}_{t-2}\}, \mathbf{J}, \hat{\mathbf{J}}, \{\hat{\mathbf{P}}\}, x) &= \sum_{s^{t-2}} \mathbf{P}_{t-2}(s^{t-2}) \\ &\times \sum_{s_1^{t-1}, \dots, s_k^{t-1}} W(s^t | \sum_{j=1}^k J_j s_j^{t-1} + x) \prod_{j=1}^k \hat{\mathbf{P}}_j(s_j^{t-1}). \end{aligned} \quad (50)$$

Equations (47) and (49) can be solved by a population dynamics procedure [25, 39]. In figure 12 we show the cumulative distribution function of site activation probabilities $P(\langle s(t) \rangle) = \pi(P(s^t = 1))$ at different times, computed solving the above equations via population dynamics, for a random regular graph with fully symmetric interactions. We find reasonable agreement with MC simulations on a single instance of a network with size $N = 10^4$. We however, see small deviations due to the cavity equations in this instance being averaged over the disorder $P(\mathbf{J})$. As expected from earlier analysis in Sec. 4 the time-dependent distribution of activation probabilities reaches a multi-modal steady-state.

7. Discussion

In our work we have studied systems of sparsely connected Boolean variables with multi-node and self-interactions. Previous work has shown that self-interactions complicate the analysis of dynamics. However, by mapping to an equivalent bipartite system, we find that the dynamical cavity method, within a OTA scheme, provides an efficient numerical framework to study the dynamics of systems with arbitrary bidirectionality, multi-node and self-interactions. We have shown for such systems that the OTA scheme predicts the activation probability of each site in the transient and non-equilibrium steady-state, down to relatively low temperature, where the system is ergodic. As temperature is lowered further, ergodicity is eventually broken, and we have found that the error increases with the bidirectionality of the interactions. At zero

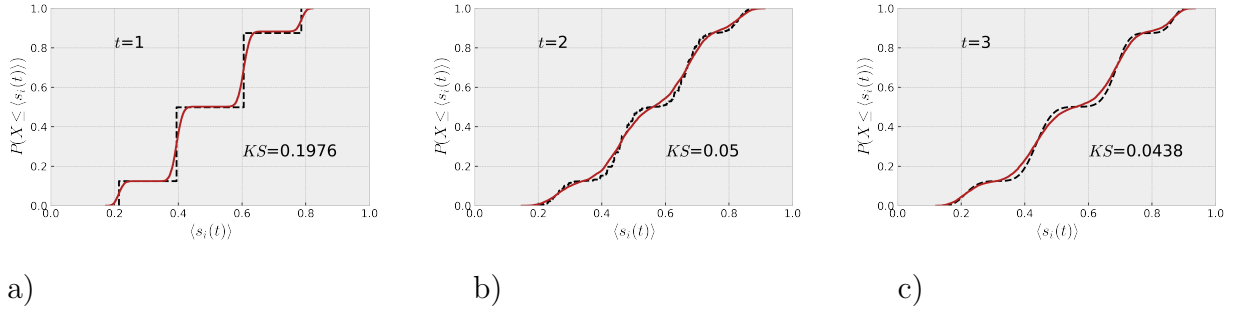


Figure 12. CDF of activation probabilities for the Boolean system defined in (5) at time $t = 1, 2, 3$ (from (a) to (c)). The network is a random regular graph with degree $c = 3$. Interactions are fully symmetric, i.e. $J_{ij} = J_{ji}$ and are drawn from the set $\{-1, 1\}$ with equal probability. Self-interactions are absent i.e. $J_{ii} = 0 \forall i$. The inverse temperature is $\beta = 1$ and initial conditions are set to $P(s_i^t) = 0.5 \forall i$. Dashed line indicates solution to equation (47) from population dynamics with sample size $S = 2.5 \times 10^5$. Solid line indicates results from MC simulations for a network of size $N = 10^4$. Annotations indicate the Kolmogorov–Smirnov (KS) statistic comparing the empirical distributions from the cavity method and MC simulations.

temperature, however, if the dynamical cavity is given the same initial configuration as MC simulations, the OTA scheme is in excellent agreement with simulations, showing that OTA accurately describes the dynamics within any given ergodic sector. We have also derived equations for the distribution (and mean) of site activations at a given time, in the thermodynamic limit, within a OTA scheme, which is numerically more efficient than previous approaches involving sums over the history of a trajectory [14]. We comment that these equations, when compared to their analogue derived by generating functionals [37, 38] provide physical insight into the effect of truncating memory terms in the GFA. In principle, the dynamical cavity equations are also solvable for networks with strong degree correlations, as shown in previous work [39]. By providing closed expressions for the distribution of site marginals, the dynamical cavity method can provide insight into the heterogeneity of site trajectories for a typical network drawn from some ensemble. This is unlike GFA which only provides information on the trajectory of a typical site.

From our work, it is clear that sparse networks with partially bidirectional interactions support multiple (cyclic) attractors, at low noise. Additionally, multi-node interactions are found to decrease the overlap between attractors, suggesting that cooperativity increases diversification of attractors. The existence of a multiplicity of attractors in partially bidirectional sparse systems is an important feature for models of GRNs to sustain multi-cellular life. It means that if a GRN is in an attractor, it can be pushed out of this attractor by some event, for example the sudden change in external field, and can move from one attractor to another. This could describe how cells move from one cell type to another. Both cooperative effects and gene self-regulation (i.e. a gene coding for a TF that regulates the gene itself) are commonly observed in GRNs and our work suggests that it is these features in combination which allow GRNs to support

a diverse set of stable gene expression profiles, corresponding to different cell types, with self-regulation playing an important role in determining the nature of attractors.

Our work poses interesting questions for future work. One point of focus would be to study how a GRN may move from one attractor to another, either by the application of time-dependent external fields, or dynamic variations in the interaction network itself. One could also focus on adding prescribed degree sequences to impose structure that is a more realistic description of GRNs. Of course while we can deduce that a multiplicity of (cyclic) attractors exist, it remains an open question how the attractors relate to the specific realisation of the bipartite network. An analytical framework to deduce the number of attractors that are supported by a network also remains an open point of investigation. Our work also suggests that there is an ergodicity breaking phase at low temperatures characterised by an overlap distribution which resembles the one observed in equilibrium spin systems (with symmetric interactions and fixed-point attractors) exhibiting one step of replica symmetry breaking. Due to the arbitrary symmetry of the interactions, however, this would have to be formally ascertained by as yet unknown dynamical methods. Such methods will be necessary to advance our understanding of sparse systems with multi-node interactions out of equilibrium and may give further insight into the behaviour of GRNs.

Acknowledgments

CJH is supported by the EPSRC Centre for Doctoral Training in Cross-Disciplinary Approaches to Non-Equilibrium Systems (CANES, EP/L015854/1). AA wishes to thank the Chimera group at the University of Rome, Sapienza, for the kind hospitality.

Appendix A. Dynamical cavity approach to bipartite systems

We show here how the dynamical cavity method may be used to analyse the dynamics of the general bipartite system defined in (9) and (10), from which the linear model with self-interactions (5) and the nonlinear model with multi-node interactions (6) may be recovered by suitable choice of parameters. Starting with equation (11), we wish to derive a closed set of equations for single site quantities at a given time, like s_i^t and τ_μ^t . To do so, we first consider the trajectory of a single gene i ,

$$P_i(s_i^{0\dots t_m}) = \sum_{\mathbf{s}^{0\dots t_m} \setminus s_i^{0\dots t_m}, \boldsymbol{\tau}^{0\dots t_m}} P(\mathbf{s}^{0\dots t_m}, \boldsymbol{\tau}^{0\dots t_m}). \quad (\text{A.1})$$

As is typical of the dynamical cavity formalism, we assume that the bipartite network has the topological structure of a tree and that initial conditions factorise over the sites of the tree $P(\mathbf{s}^0, \boldsymbol{\tau}^0) = \prod_{i\mu} P(s_i^0, \tau_\mu^0)$. In doing so we can rewrite the equation above as

follows,

$$\begin{aligned}
 P_i(s_i^{0\dots t_m}) &= \sum_{\mathbf{s}^{0\dots t_m} \setminus s_i^{0\dots t_m}, \boldsymbol{\tau}^{0\dots t_m}} P(\mathbf{s}^0, \boldsymbol{\tau}^0) \left[\prod_{t=1}^{t_m} W(s_i^t | h_i(\boldsymbol{\tau}_{\partial_i}^{t-1})) \prod_{j \in T_i \setminus i} W(s_j^t | h_j(\boldsymbol{\tau}_{\partial_j}^{t-1})) \right] \\
 &\quad \times \prod_{\mu \in \partial_i} \left[\prod_{t=1}^{t_m} \widetilde{W}(\tau_\mu^t | h_\mu(\mathbf{s}_{\partial_\mu}^{t-1})) \prod_{\nu \in T_\mu \setminus \mu} \widetilde{W}(\tau_\nu^t | h_\nu(\mathbf{s}_{\partial_\nu}^{t-1})) \right] \\
 &= \sum_{\mathbf{s}^{0\dots t_m} \setminus s_i^{0\dots t_m}, \boldsymbol{\tau}^{0\dots t_m}} P(\mathbf{s}^0, \boldsymbol{\tau}^0) \left[\prod_{t=1}^{t_m} W(s_i^t | h_i(\boldsymbol{\tau}_{\partial_i}^{t-1})) \right] \\
 &\quad \times \prod_{\mu \in \partial_i} \left[\prod_{t=1}^{t_m} \widetilde{W}(\tau_\mu^t | h_\mu(\mathbf{s}_{\partial_\mu}^{t-1})) \prod_{\nu, j \in T_\mu \setminus \mu, i} \widetilde{W}(\tau_\nu^t | h_\nu(\mathbf{s}_{\partial_\nu}^{t-1})) W(s_j^t | h_j(\boldsymbol{\tau}_{\partial_j}^{t-1})) \right] \\
 &= P(s_i^0) \sum_{\boldsymbol{\tau}_{\partial_i}^{0\dots t_m}} \left[\prod_{t=1}^{t_m} W(s_i^t | h_i(\boldsymbol{\tau}_{\partial_i}^{t-1})) \right] \prod_{\mu \in \partial_i} \left\{ \sum_{\mathbf{s}_{T_\mu \setminus i}^{0\dots t_m}, \boldsymbol{\tau}_{T_\mu \setminus \mu}^{0\dots t_m}} P(\mathbf{s}_{T_\mu}^0 \setminus s_i^0) P(\boldsymbol{\tau}_{T_\mu}^0) \right. \\
 &\quad \left. \times \left[\prod_{t=1}^{t_m} \widetilde{W}(\tau_\mu^t | h_\mu(\mathbf{s}_{\partial_\mu}^{t-1})) \prod_{\nu, j \in T_\mu \setminus \mu, i} \widetilde{W}(\tau_\nu^t | h_\nu(\mathbf{s}_{\partial_\nu}^{t-1})) W(s_j^t | h_j(\boldsymbol{\tau}_{\partial_j}^{t-1})) \right] \right\} \quad (\text{A.2})
 \end{aligned}$$

where we have defined $\mathbf{s}_{T_\mu} = \{s_i, i \in T_\mu\}$ and $\boldsymbol{\tau}_{T_\mu} = \{\tau_\nu, \nu \in T_\mu\}$ where T_μ and T_i are trees rooted at nodes μ and i . We may then take the external sum over $\boldsymbol{\tau}_{\partial_i}^{t_m}$ and the internal sums over $\boldsymbol{\tau}_{T_\mu}^{t_m}$ and $\mathbf{s}_{T_\mu}^{t_m}$,

$$\begin{aligned}
 P_i(s_i^{0\dots t_m}) &= P(s_i^0) \sum_{\boldsymbol{\tau}_{\partial_i}^{0\dots t_m-1}} \left[\prod_{t=1}^{t_m} W(s_i^t | h_i(\boldsymbol{\tau}_{\partial_i}^{t-1})) \right] \prod_{\mu \in \partial_i} \left\{ \sum_{\mathbf{s}_{T_\mu \setminus i}^{0\dots t_m-1}, \boldsymbol{\tau}_{T_\mu \setminus \mu}^{0\dots t_m-1}} P(\mathbf{s}_{T_\mu}^0 \setminus s_i^0) \right. \\
 &\quad \left. \times P(\boldsymbol{\tau}_{T_\mu}^0) \left[\prod_{t=1}^{t_m-1} \widetilde{W}(\tau_\mu^t | h_\mu(\mathbf{s}_{\partial_\mu}^{t-1})) \prod_{\nu, j \in T_\mu \setminus \mu, i} \widetilde{W}(\tau_\nu^t | h_\nu(\mathbf{s}_{\partial_\nu}^{t-1})) W(s_j^t | h_j(\boldsymbol{\tau}_{\partial_j}^{t-1})) \right] \right\}. \quad (\text{A.3})
 \end{aligned}$$

We note that the local field that acts on TF μ can be written as,

$$h_\mu(\mathbf{s}_{\partial_\mu}^{t-1}) = \sum_{j \in \partial_\mu \setminus i} \eta_j^\mu s_j^{t-1} + \vartheta_\mu + \eta_i^\mu s_i^{t-1} = h_\mu^{(i)}(\mathbf{s}_{\partial_\mu}^{t-1}) + \zeta_\mu^{(i),t} \quad (\text{A.4})$$

where we have defined the local field in a new copy of the network where site i is removed, referred to as the *cavity graph*, $h_\mu^{(i)}(\mathbf{s}_{\partial_\mu}^{t-1}) = \sum_{j \in \partial_\mu \setminus i} \eta_j^\mu s_j^{t-1} + \vartheta_\mu$, and the time dependent external field $\zeta_\mu^{(i),t} = \eta_i^\mu s_i^{t-1}$, which is the effect of the removed gene i on TF μ in the cavity graph. Similarly, we can write the local field that acts on gene i as,

$$h_i(\boldsymbol{\tau}_{\partial_i}^{t-1}) = \sum_{\mu \in \partial_i \setminus \nu} \xi_i^\mu \tau_\mu^{t-1} + \vartheta_i + \xi_i^\nu \tau_\nu^{t-1} = h_i^{(\nu)}(\boldsymbol{\tau}_{\partial_i}^{t-1}) + \zeta_i^{(\nu),t} \quad (\text{A.5})$$

denoting the local field in the cavity graph where TF ν is removed, $h_i^{(\nu)}(\boldsymbol{\tau}_{\partial_i}^{t-1}) = \sum_{\mu \in \partial_i \setminus \nu} \xi_i^\mu \tau_\mu^{t-1} + \vartheta_i$, and external field $\zeta_i^{(\nu),t} = \xi_i^\nu \tau_\nu^{t-1}$. We can then define the contents of

the curly brackets in equation (A.3) as $P_\mu^{(i)}(\tau_\mu^{0\dots t_m-1}|\zeta_\mu^{(i),1\dots t_m-1})$, which is the probability to observe the trajectory $\tau_\mu^{0\dots T-1}$ in the cavity graph where gene i is removed, given that the time dependent external field, $\zeta_\mu^{(i),1\dots t_m}$, acts on TF μ . With this definition in place, equation (A.3) is now equivalent to

$$P_i(s_i^{0\dots t_m}) = P(s_i^0) \sum_{\tau_{\partial_i}^{0\dots t_m-1}} \left[\prod_{t=1}^{t_m} W(s_i^t|h_i(\tau_{\partial_i}^{t-1})) \right] \prod_{\mu \in \partial_i} P_\mu^{(i)}(\tau_\mu^{0\dots t_m-1}|\zeta_\mu^{(i),1\dots t_m-1}). \quad (\text{A.6})$$

Following the same reasoning, we can derive an analogous expression for the trajectory of a single TF μ ,

$$P_\mu(\tau_\mu^{0\dots t_m}) = P(\tau_\mu^0) \sum_{\mathbf{s}_{\partial_\mu}^{0\dots t_m-1}} \left[\prod_{t=1}^{t_m} \widetilde{W}(\tau_\mu^t|h_\mu(\mathbf{s}_{\partial_\mu}^{t-1})) \right] \prod_{j \in \partial_\mu} P_j^{(\mu)}(s_j^{0\dots t_m-1}|\zeta_j^{(\mu),1\dots t_m-1}) \quad (\text{A.7})$$

where $P_j^{(\mu)}(s_j^{0\dots t_m-1}|\zeta_j^{(\mu),1\dots t_m-1})$ is the probability to observe the trajectory $s_j^{0\dots t_m-1}$ in the cavity graph where site μ is removed, given that the time-dependent external field $\zeta_j^{(\mu),1\dots t_m-1} = \xi_j^\mu \tau_\mu^{1\dots t_m-1}$, acts on site j . Equations for the probability to observe the trajectory of a single gene i in the *cavity graph* are found by considering the effect of removing TF ν from equation (A.6),

$$P_i^{(\nu)}(s_i^{0\dots t_m}) = P(s_i^0) \sum_{\tau_{\partial_i \setminus \nu}^{0\dots t_m-1}} \left[\prod_{t=1}^{t_m} W(s_i^t|h_i^{(\nu)}(\tau_{\partial_i}^{t-1})) \right] \prod_{\mu \in \partial_i \setminus \nu} P_\mu^{(i)}(\tau_\mu^{0\dots t_m-1}|\zeta_\mu^{(i),1\dots t_m-1}), \quad (\text{A.8})$$

which depends upon the cavity field $h_i^{(\nu)}(\tau_{\partial_i}^{t-1})$. Similarly, by removing gene ℓ from equation (A.7) we find,

$$P_\mu^{(\ell)}(\tau_\mu^{0\dots t_m}) = P(\tau_\mu^0) \sum_{\mathbf{s}_{\partial_\mu \setminus \ell}^{0\dots t_m-1}} \left[\prod_{t=1}^{t_m} \widetilde{W}(\tau_\mu^t|h_\mu^{(\ell)}(\mathbf{s}_{\partial_\mu}^{t-1})) \right] \prod_{j \in \partial_\mu \setminus \ell} P_j^{(\mu)}(s_j^{0\dots t_m-1}|\zeta_j^{(\mu),1\dots t_m-1}), \quad (\text{A.9})$$

which depends upon the cavity field $h_\mu^{(\ell)}(\mathbf{s}_{\partial_\mu}^{t-1})$. If we now consider an external field $\zeta_i^{(\nu),1\dots t_m}$ acting on gene i in the cavity graph with TF ν removed, the cavity field in equation (A.8) will become $h_i^{(\nu)}(\tau_{\partial_i}^{t-1}) + \zeta_i^{(\nu),t} = h_i(\tau_{\partial_i}^{t-1})$, from which we deduce equation (14). Similarly, if an external field $\zeta_\mu^{(\ell),1\dots t_m}$ acts on TF μ in the cavity graph where gene ℓ is removed, from equation (A.8), we can deduce equation (15). We have derived a closed system of equations (A.6), (A.7), (14) and (15) which in principle can be solved recursively for the trajectory of the system. As noted in the main text, their computational complexity grows exponentially with the length of the trajectory.

If we assume that the system has unidirectional interactions, however, the cavity equations simplify. In this case, $\xi_i^\mu \neq 0$ implies $\eta_i^\mu = 0$, such that the external fields

in equation (A.6) vanish, $\zeta_\mu^{(i),t} = 0$, and the RHS of equations (A.7) and (15) become identical, as $\ell \notin \partial_\mu$ when $\mu \in \partial_\ell$ and given (A.4) we have $P_\mu^{(i)}(\tau_\mu^{0\dots t_m} | 0) = P_\mu(\tau_\mu^{0\dots t_m})$. This simplifies equation (A.6) to

$$P_i(s_i^{0\dots t_m}) = P(s_i^0) \sum_{\tau_{\partial_i}^{0\dots t_m-1}} \left[\prod_{t=1}^{t_m} W(s_i^t | h_i(\tau_{\partial_i}^{t-1})) \right] \prod_{\mu \in \partial_i} P_\mu(\tau_\mu^{0\dots t_m-1}) \quad (\text{A.10})$$

and by the same argument one can also derive the trajectory for the TFs,

$$P_\mu(\tau_\mu^{0\dots t_m}) = P(\tau_\mu^0) \sum_{\mathbf{s}_{\partial_\mu}^{0\dots t_m-1}} \left[\prod_{t=1}^{t_m} \widetilde{W}(\tau_\mu^t | h_\mu(\mathbf{s}_{\partial_\mu}^{t-1})) \right] \prod_{j \in \partial_\mu} P_j(s_j^{0\dots t_m-1}). \quad (\text{A.11})$$

We may now marginalise equation (A.10) over $s_i^{0\dots t_m-1}$ and equation (A.11) over $\tau_\mu^{0\dots t_m-1}$ and find,

$$P_i(s_i^{t_m}) = \sum_{\tau_{\partial_i}^{t_m-1}} [W(s_i^{t_m} | h_i(\tau_{\partial_i}^{t_m-1}))] \prod_{\mu \in \partial_i} P_\mu(\tau_\mu^{t_m-1}) \quad (\text{A.12})$$

$$P_\mu(\tau_\mu^{t_m}) = \sum_{\mathbf{s}_{\partial_\mu}^{t_m-1}} [\widetilde{W}(\tau_\mu^{t_m} | h_\mu(\mathbf{s}_{\partial_\mu}^{t_m-1}))] \prod_{j \in \partial_\mu} P_j(s_j^{t_m-1}). \quad (\text{A.13})$$

Equations (A.12) and (A.13) are a closed set of equations which may be solved by simple iteration. They reveal that in systems with unidirectional interactions, $P(s_{\partial_\mu}^t) = \prod_{j \in \partial_\mu} P_j(s_j^t)$.

As we note in Sec. 3, for systems with arbitrarily bidirectional interactions, we may use the OTA scheme to reduce the time complexity of the cavity equations, which in the case of our bipartite system means to assume (16) and (17). If we insert (17) into (14) and isolate the terms which contain s_i^T and $\tau_{\partial_i}^{T-1}$, we can rewrite the RHS in terms of the cavity distribution of the s_i trajectory up until time $t_m - 1$,

$$\begin{aligned} P_i^{(\nu)}(s_i^{0\dots t_m} | \zeta_i^{(\nu), 1\dots t_m}) &= P(s_i^0) \sum_{\tau_{\partial_i \setminus \nu}^{0\dots t_m-1}} \left[\prod_{t=1}^{t_m} W(s_i^t | h_i(\tau_{\partial_i}^{t-1})) \right] \prod_{\mu \in \partial_i \setminus \nu} P_\mu(\tau_\mu^0) \prod_{t=1}^{t_m-1} P_\mu^{(i)}(\tau_\mu^t | \zeta_\mu^{(i), t}) \\ &= \sum_{\tau_{\partial_i \setminus \nu}^{t_m-1}} W(s_i^{t_m} | h_i(\tau_{\partial_i}^{t_m-1})) \left[\prod_{\mu \in \partial_i \setminus \nu} P_\mu^{(i)}(\tau_\mu^{t_m-1} | \zeta_\mu^{(i), t_m-1}) \right] P(s_i^0) \\ &\quad \times \sum_{\tau_{\partial_i}^{0\dots t_m-2}} \left[\prod_{t=1}^{t_m-1} W(s_i^t | h_i(\tau_{\partial_i}^{t-1})) \right] \prod_{\mu \in \partial_i \setminus \nu} P_\mu(\tau_\mu^0) \prod_{t=1}^{t_m-2} P_\mu^{(i)}(\tau_\mu^t | \zeta_\mu^{(i), t}) \\ &= \sum_{\tau_{\partial_i \setminus \nu}^{t_m-1}} W(s_i^{t_m} | h_i(\tau_{\partial_i}^{t_m-1})) \left[\prod_{\mu \in \partial_i \setminus \nu} P_\mu^{(i)}(\tau_\mu^{t_m-1} | \zeta_\mu^{(i), t_m-1}) \right] \\ &\quad \times P_i^{(\nu)}(s_i^{0\dots t_m-1} | \zeta_i^{(\nu), 1\dots t_m-1}). \end{aligned} \quad (\text{A.14})$$

At this stage it is possible to marginalise the above over s_i^{0,\dots,t_m-1} ,

$$\begin{aligned}
 P_i(s_i^{t_m} | \zeta_i^{(\nu),1\dots t_m}) &= \sum_{s_i^{0\dots t_m-1}} \sum_{\tau_{\partial_i \setminus \nu}^{t_m-1}} W(s_i^{t_m} | h_i(\tau_{\partial_i}^{t_m-1})) \left[\prod_{\mu \in \partial_i \setminus \nu} P_\mu^{(i)}(\tau_\mu^{t_m-1} | \zeta_\mu^{(i),t_m-1}) \right] \\
 &\times P_i^{(\nu)}(s_i^{0\dots t_m-1} | \zeta_i^{(\nu),1\dots t_m-1}) \\
 &= \sum_{s_i^{0\dots t_m-1}} \sum_{\tau_{\partial_i \setminus \nu}^{t_m-1}} W(s_i^{t_m} | h_i(\tau_{\partial_i}^{t_m-1})) \left[\prod_{\mu \in \partial_i \setminus \nu} P_\mu^{(i)}(\tau_\mu^{t_m-1} | \zeta_\mu^{(i),t_m-1}) \right] \\
 &\times P_i(s_i^0) \prod_{t=1}^{t_m-1} P_i^{(\nu)}(s_i^t | \zeta_i^{(\nu),t}) \\
 &= \sum_{s_i^{t_m-2}} \sum_{\tau_{\partial_i \setminus \nu}^{t_m-1}} W(s_i^{t_m} | h_i^{(\nu)}(\tau_{\partial_i}^{t_m-1}) + \zeta_i^{(\nu),t_m}) \\
 &\times \left[\prod_{\mu \in \partial_i \setminus \nu} P_\mu^{(i)}(\tau_\mu^{t_m-1} | \zeta_\mu^{(i),t_m-1}) \right] P_i^{(\nu)}(s_i^{t_m-2} | \zeta_i^{(\nu),t_m-2}). \tag{A.15}
 \end{aligned}$$

It is now apparent that the LHS only depends on $\zeta_i^{(\nu),t_m-2}$ and $\zeta_i^{(\nu),t_m}$ i.e $P_i(s_i^{t_m} | \zeta_i^{(\nu),1\dots t_m}) = P_i(s_i^{t_m} | \zeta_i^{(\nu),t_m-2,t_m})$, such that we can write

$$\begin{aligned}
 P_i^{(\nu)}(s_i^{t_m} | \zeta_i^{(\nu),t_m-2,t_m}) &= \sum_{s_i^{t_m-2}} \sum_{\tau_{\partial_i \setminus \nu}^{t_m-1}} W(s_i^{t_m} | h_i^{(\nu)}(\tau_{\partial_i}^{t_m-1}) + \zeta_i^{(\nu),t_m}) \\
 &\times \left[\prod_{\mu \in \partial_i \setminus \nu} P_\mu^{(i)}(\tau_\mu^{t_m-1} | \zeta_\mu^{(i),t_m-1}) \right] P_i^{(\nu)}(s_i^{t_m-2} | \zeta_i^{(\nu),t_m-2}). \tag{A.16}
 \end{aligned}$$

In principle, this is in contradiction with the Markovian assumption made for the cavity distribution, which would require $P_i^{(\nu)}(s_i^{t_m} | \zeta_i^{(\nu),t_m-2,t_m}) = P_i^{(\nu)}(s_i^{t_m} | \zeta_i^{(\nu),t_m})$. Such inconsistency arises from treating a non-Markovian process as Markovian. In order to get a closed set of equations for the one-time cavity marginal, further closure assumptions are thus required. As stated in Sec. 3, we assume that the cavity distribution, with external field from the removed site, may be approximated by its non-cavity counterpart i.e $P_i^{(\nu)}(s_i^{t_m-2} | \zeta_i^{(\nu),t_m-2}) \approx P_i(s_i^{t_m-2})$, following [17]. Under this approximation, from (A.16) we retrieve equation (18), and by considering adding the removed TF ν back in and setting external fields to zero, we find, for the non-cavity distribution, the expression given in (22). By the same reasoning, we can derive analogous equations for the trajectory of a TF μ . In summary, the dynamics of the bipartite system are fully described, under the OTA scheme, by the closed, coupled set of equations (18),(19),(22) and (23), which can be solved by iteration given some initial conditions $P_i(s_i^0)$ and $P_\mu(\tau_\mu^0)$.

Appendix B. Equilibrium analysis of (0,1) spins with parallel update and self-interactions

In this appendix we use the cavity method to calculate the equilibrium value of site marginals for the linear threshold model (5) with self-interactions. Assuming that $z_i(t)$ is a random variable with c.d.f. (2), we can write the evolution of the state probability as a Markov chain

$$P_{t+1}(\mathbf{s}) = \sum_{\mathbf{s}'} W(\mathbf{s}|\mathbf{s}') P_t(\mathbf{s}') \quad (\text{B.1})$$

with transition probability

$$W(\mathbf{s}|\mathbf{s}') = \prod_{i=1}^N W(s_i|h_i(\mathbf{s}'_{\partial_i}, s'_i)) = \prod_{i=1}^N \frac{e^{\frac{\beta}{2}(2s_i-1)h_i(\mathbf{s}'_{\partial_i}, s'_i)}}{2 \cosh \frac{\beta}{2} h_i(\mathbf{s}'_{\partial_i}, s'_i)}, \quad (\text{B.2})$$

where $h_i(\mathbf{s}_{\partial_i}, s_i) = \sum_{j \in \partial_i} J_{ij} s_j + J_{ii} s_i + \vartheta_i$. If the interactions are fully symmetric, $J_{ij} = J_{ji}$, the transition probabilities (B.2) satisfy detailed balance

$$p_{\text{eq}}(\mathbf{s}) W(\mathbf{s}'|\mathbf{s}) = p_{\text{eq}}(\mathbf{s}') W(\mathbf{s}|\mathbf{s}') \quad (\text{B.3})$$

with the equilibrium distribution

$$p_{\text{eq}}(\mathbf{s}) = \frac{1}{Z} e^{-\beta H_\beta(\mathbf{s})} \quad (\text{B.4})$$

where $H_\beta(\mathbf{s}) = -\frac{1}{\beta} \sum_i \ln 2 \cosh \frac{\beta}{2} h_i(\mathbf{s}_{\partial_i}, s_i) - \frac{1}{2} \sum_i h_i(\mathbf{s}_{\partial_i}, s_i) - \sum_i s_i \vartheta_i$. We can rewrite this distribution in a form more amenable to analysis if we consider a fictitious set of variables $\boldsymbol{\tau} = \{0, 1\}^N$,

$$p_{\text{eq}}(\mathbf{s}) = \frac{1}{Z} \prod_{i=1}^N 2 \cosh \frac{\beta}{2} h_i(\mathbf{s}_{\partial_i}, s_i) e^{\frac{\beta}{2} h_i(\mathbf{s}_{\partial_i}, s_i)} e^{\beta \vartheta_i s_i} \quad (\text{B.5})$$

$$= \frac{1}{Z} \prod_{i=1}^N \sum_{\tau_i} e^{\frac{\beta}{2}(2\tau_i-1)h_i(\mathbf{s}_{\partial_i}, s_i)} e^{\frac{\beta}{2} h_i(\mathbf{s}_{\partial_i}, s_i)} e^{\beta \vartheta_i s_i} \quad (\text{B.6})$$

where we have used $2 \cosh(x) = \sum_{\tau \in \{0,1\}} e^{(2\tau-1)x}$ as in [23, 24]. The equilibrium distribution can then be written as

$$p_{\text{eq}}(\mathbf{s}) = \frac{1}{Z} \sum_{\boldsymbol{\tau}} e^{\beta \sum_{i \neq j} \tau_i J_{ij} s_j + \beta \sum_i \tau_i J_{ii} s_i + \beta \sum_i \vartheta_i (s_i + \tau_i)}. \quad (\text{B.7})$$

the marginalisation of the joint distribution of real and fictitious variables (26).

Now we use the cavity method to find a closed set of equations for single site quantities. To do so we marginalise (26) over all sites except i ,

$$p_i(s_i, \tau_i) = \frac{1}{Z} \sum_{\mathbf{s} \setminus s_i} \sum_{\boldsymbol{\tau} \setminus \tau_i} e^{-\beta \mathcal{H}(\mathbf{s}, \boldsymbol{\tau})} \quad (\text{B.8})$$

and note that the Hamiltonian can be written in the form $\mathcal{H}(\mathbf{s}, \boldsymbol{\tau}) = -s_i h_i(\boldsymbol{\tau}_{\partial_i}) - \tau_i h_i(\mathbf{s}_{\partial_i}) - s_i J_{ii} \tau_i - \vartheta_i(\tau_i + s_i) + \mathcal{H}^{(i)}(\mathbf{s}, \boldsymbol{\tau})$ where we have defined the Hamiltonian of the system where site i has been removed $\mathcal{H}^{(i)}(\mathbf{s}, \boldsymbol{\tau}) = -\sum_{\ell \neq (i,j)} s_\ell J_{\ell j} \tau_j - \sum_{\ell \neq i} s_\ell J_{\ell} \tau_\ell - \sum_{\ell \neq i} \vartheta_\ell(s_\ell + \tau_\ell)$. With this definition the site marginal may be written in the following form,

$$p_i(s_i, \tau_i) = \frac{1}{Z_i} \sum_{\boldsymbol{\tau}_{\partial_i}} e^{\beta(s_i h_i(\boldsymbol{\tau}_{\partial_i}) + \tau_i h_i(\mathbf{s}_{\partial_i}) + s_i J_{ii} \tau_i + \vartheta_i(s_i + \tau_i))} p^{(i)}(\mathbf{s}_{\partial_i}, \boldsymbol{\tau}_{\partial_i}) \quad (\text{B.9})$$

where $p^{(i)}(\mathbf{s}_{\partial_i}, \boldsymbol{\tau}_{\partial_i})$ is the equilibrium distribution of the neighbours of site i , in the cavity graph where i is removed, $Z^{(i)} = \sum_{\mathbf{s} \setminus s_i} \sum_{\boldsymbol{\tau} \setminus \tau_i} e^{-\beta \mathcal{H}^{(i)}(\mathbf{s}, \boldsymbol{\tau})}$ is its corresponding partition function and $Z_i = Z/Z^{(i)}$. The cavity approach assumes that cavity fields are independent of each other, such that $p^{(i)}(\mathbf{s}_{\partial_i}, \boldsymbol{\tau}_{\partial_i}) = \prod_{j \in \partial_i} p_j^{(i)}(s_j, \tau_j)$, which is exact on trees and sparse graphs which are locally tree-like in the limit $N \rightarrow \infty$. Under this assumption the site marginals and cavity site marginals can be found from the closed set of equations (27) and (28). In order to solve these equations, it is convenient to parameterise the cavity marginals in terms of effective fields

$$p_i^{(\ell)}(s_i, \tau_i) = \frac{1}{Z_i^{(\ell)}} e^{\frac{\beta}{2}((2s_i-1)h_{i\ell}^s + (2\tau_i-1)h_{i\ell}^\tau + (2s_i-1)(2\tau_i-1)h_{i\ell}^{s\tau})} \quad (\text{B.10})$$

and use (28) to obtain a closed set of equations for the cavity fields,

$$\begin{aligned} h_{i\ell}^s &= \frac{1}{2\beta} \sum_{j \in \partial_i \setminus \ell} \ln \left(\frac{f_{ij}(1,1)f_{ij}(1,0)}{f_{ij}(0,1)f_{ij}(0,0)} \right) + \frac{1}{2} J_{ii} + \vartheta_i \\ h_{i\ell}^\tau &= \frac{1}{2\beta} \sum_{j \in \partial_i \setminus \ell} \ln \left(\frac{f_{ij}(1,1)f_{ij}(0,1)}{f_{ij}(1,0)f_{ij}(0,0)} \right) + \frac{1}{2} J_{ii} + \vartheta_i \\ h_{i\ell}^{s\tau} &= \frac{1}{2\beta} \sum_{j \in \partial_i \setminus \ell} \ln \left(\frac{f_{ij}(1,1)f_{ij}(0,0)}{f_{ij}(0,1)f_{ij}(1,0)} \right) + \frac{1}{2} J_{ii}, \end{aligned} \quad (\text{B.11})$$

where we define,

$$f_{ij}(s_i, \tau_i) = \sum_{s_j} \sum_{\tau_j} e^{\beta(s_i J_{ij} \tau_j + \tau_i J_{ij} s_j)} p_j^{(i)}(s_j, \tau_j). \quad (\text{B.12})$$

These equations may be solved by simple iteration from some random initial condition. We can similarly parameterise the single site marginal as

$$p_i(s_i, \tau_i) = \frac{1}{Z_i} e^{\frac{\beta}{2}((2s_i-1)h_i^s + (2\tau_i-1)h_i^\tau + (2s_i-1)(2\tau_i-1)h_i^{s\tau})} \quad (\text{B.13})$$

from which one finds,

$$\begin{aligned} h_i^s &= \frac{1}{2\beta} \sum_{j \in \partial_i} \ln \left(\frac{f_{ij}(1,1)f_{ij}(1,0)}{f_{ij}(0,1)f_{ij}(0,0)} \right) + \frac{1}{2} J_{ii} + \vartheta_i \\ h_i^\tau &= \frac{1}{2\beta} \sum_{j \in \partial_i} \ln \left(\frac{f_{ij}(1,1)f_{ij}(0,1)}{f_{ij}(1,0)f_{ij}(0,0)} \right) + \frac{1}{2} J_{ii} + \vartheta_i \\ h_i^{s\tau} &= \frac{1}{2\beta} \sum_{j \in \partial_i} \ln \left(\frac{f_{ij}(1,1)f_{ij}(0,0)}{f_{ij}(0,1)f_{ij}(1,0)} \right) + \frac{1}{2} J_{ii}. \end{aligned} \quad (\text{B.14})$$

One must solve equations (B.11) by iteration, and then substitute this solution into equations (B.14) to find the fields h_i^s , h_i^τ and $h_i^{s\tau}$ from which one can find the average activation probability, $\langle s_i \rangle = \sum_{s_i, \tau_i} s_i p_i(s_i, \tau_i)$, from the following expression

$$\langle s_i \rangle = \frac{1}{Z_i} e^{\frac{\beta}{2} h_i^s} \cosh \frac{\beta}{2} (h_i^\tau + h_i^{s\tau}), \quad (\text{B.15})$$

where we have defined the normalisation constant

$$Z_i = \sum_{s_i, \tau_i} e^{\frac{\beta}{2} ((2s_i-1)h_i^s + (2\tau_i-1)h_i^\tau + (2s_i-1)(2\tau_i-1)h_i^{s\tau})}. \quad (\text{B.16})$$

Appendix C. Dynamical cavity approach to systems with self-interactions

Here we detail the dynamical cavity approach for a system of N Boolean variables with pairwise as well as self- interactions, which evolves in time according to equation (B.1). As we shall show, it is possible to derive a closed set of equations for such systems but, even for systems with unidirectional interactions, these equations are exponential in complexity, and can not be simplified using OTA schemes. To begin, we consider the trajectory of the system from time $t = 0$ to $t = t_m$, $\mathbf{s}^0 \rightarrow \mathbf{s}^1 \rightarrow \dots \rightarrow \mathbf{s}^{t_m}$, which we denote $\mathbf{s}^{0\dots t_m}$. From equation (B.1) the trajectory of the system follows,

$$P(\mathbf{s}^{0\dots t_m}) = P_0(\mathbf{s}^0) \prod_{t=1}^{t_m} W(\mathbf{s}^t | \mathbf{s}^{t-1}). \quad (\text{C.1})$$

We now assume that the interactions, due to their sparsity, are represented by a network with the topology of a tree. By following steps in Appendix A, now applied to a monopartite system, we may write the probability to observe a single site trajectory as,

$$\begin{aligned} P_i(s_i^{0\dots t_m}) &= P_i(s_i^0) \sum_{\mathbf{s}_{\partial_i}^{0\dots t_m-1}} \left[\prod_{t=1}^{t_m} W(s_i^t | h_i(\mathbf{s}_{\partial_i}^{t-1}, s_i^{t-1})) \right] \\ &\times \prod_{j \in \partial_i} P_j^{(i)}(s_j^{0\dots t_m-1} | \zeta_j^{(i), 1\dots t_m-1}) \end{aligned} \quad (\text{C.2})$$

where $P_j^{(i)}(s_j^{0\dots t_m-1} | \zeta_j^{(i), 1\dots t_m-1})$ is the probability to observe the trajectory $s_j^{0\dots t_m-1}$ in the cavity graph where site i has been removed, given that site j feels a time dependent external field $\zeta_j^{(i), t} = J_{ji} s_i^{t-1}$. Similarly, the probability of a trajectory in the cavity graph is found to be given by,

$$\begin{aligned} P_i^{(\ell)}(s_i^{0\dots t_m} | \zeta_i^{(\ell), 1\dots t_m}) &= P_i(s_i^0) \sum_{\mathbf{s}_{\partial_i \setminus \ell}^{0\dots t_m-1}} \left[\prod_{t=1}^{t_m} W(s_i^t | h_i(\mathbf{s}_{\partial_i}^{t-1}, s_i^{t-1})) \right] \\ &\times \prod_{j \in \partial_i \setminus \ell} P_j^{(i)}(s_j^{0\dots t_m-1} | \zeta_j^{(i), 1\dots t_m-1}). \end{aligned} \quad (\text{C.3})$$

We are interested in the site marginals at a given time, however, in the presence of self-interactions, we cannot perform the sum over $s_i^{0\dots t_m-1}$ explicitly, even in the simplest scenario where interactions are unidirectional, as we will show explicitly below. As noted earlier, for unidirectional interactions, cavity and non-cavity distributions are equal, so we can write

$$\begin{aligned} P_i(s_i^{0\dots t_m}) &= P_i(s_i^0) \sum_{\mathbf{s}_{\partial_i}^{0\dots t_m-1}} \left[\prod_{t=1}^{t_m} W(s_i^t | h_i(\mathbf{s}_{\partial_i}^{t-1}, s_i^{t-1})) \right] \\ &\times \prod_{j \in \partial_i} P_j(s_j^{0\dots t_m-1}). \end{aligned} \quad (\text{C.4})$$

These equations cannot, however, be simplified by assuming suitably factorised forms of the trajectory distribution. Even if we were to assume a fully factorised distribution

$$P_j(s_j^{0\dots t_m-1}) = \prod_{t=0}^{t_m-1} P_j(s_j^t)$$

we would be left with

$$P_i(s_i^{t_m}) = \sum_{\mathbf{s}_i^{0\dots t_m-1}} P_i(s_i^0) \prod_{t=1}^{t_m} \sum_{\mathbf{s}_{\partial_i}^{t-1}} W(s_i^t | h_i(\mathbf{s}_{\partial_i}^{t-1}, s_i^{t-1})) \prod_{j \in \partial_i} P_j(s_j^{t-1}) \quad (\text{C.5})$$

which requires summing over a number $2^{t_m(1+|\partial_i|)}$ of variables which grows exponentially in time. We would thus need to face the full complexity of equations (C.2) and (C.3).

For unidirectional systems *without* self-interactions, as shown in Appendix A, it is possible to reduce the exponential complexity of the dynamical cavity equations, by deriving an expression for the single site marginal $P_i(s_i^t)$. However, here we find that one can not marginalise (C.4) over $\mathbf{s}_i^{0\dots t_m-1}$ due to the presence of self-interactions, and one is forced to consider other methods to reduce the complexity of the cavity equations. Previous works have applied the OTA scheme to systems without self-interactions, but with bidirectional interactions, where strong memory effects are present. The analogous OTA for unidirectional systems with self-interactions is applied by assuming the cavity trajectories factorise in the following way,

$$P_i^{(\ell)}(s_i^{0\dots t_m-1}) = P_i(s_i^0) \prod_{t=1}^{t_m-1} P_i^{(\ell)}(s_i^t | s_i^{t-1}) \quad (\text{C.6})$$

where we have used $P_i^{(\ell)}(s_i^0) = P_i(s_i^0)$. Inserting this into (C.3) we find,

$$\begin{aligned} P_i^{(\ell)}(s_i^{0\dots t_m}) &= P_i(s_i^0) \sum_{\mathbf{s}_{\partial_i \setminus \ell}^{0\dots t_m-1}} \left[\prod_{t=1}^{t_m} W(s_i^t | h_i(\mathbf{s}_{\partial_i}^{t-1}, s_i^{t-1})) \right] \\ &\times \prod_{j \in \partial_i \setminus \ell} P_j(s_j^0) \prod_{t=1}^{t_m-1} P_j^{(i)}(s_j^t | s_j^{t-1}). \end{aligned} \quad (\text{C.7})$$

However, we find that it is still *not* possible to marginalise (C.7) over $s_i^{0\dots t_m-1}$ without making *uncontrolled* approximations. Hence, a different procedure is necessary to solve for the dynamics of systems with self-interactions, as we detail in Sec. 4.2.

Appendix D. One time approximation in the thermodynamic limit

We now show how the distribution of site marginals for monopartite systems without self-interactions, $\pi(\{P_t\})$, defined in equation (46), may be computed from the cavity method in the limit $N \rightarrow \infty$. Starting from equation (46) we insert unity of the form,

$$\begin{aligned}
 1 = & \sum_k \delta_{k,|\partial_i|} \int \{dP_{t-2}\} \prod_{s^{t-2}} \delta(P_{t-2}(s^{t-2}) - P_i(s^{t-2})) \\
 & \times \prod_{j \in \partial_i} \left\{ \int dJ_j d\hat{J}_j \delta(J_j - J_{ij}) \delta(\hat{J}_j - J_{ji}) \right. \\
 & \left. \times \int \{d\hat{P}_j\} \prod_{s_j^{t-1}} \delta(\hat{P}_j(s_j^{t-1}) - P_j^{(i)}(s_j^{t-1} | \hat{J}_j s^{t-2})) \right\}
 \end{aligned} \tag{D.1}$$

which yields,

$$\begin{aligned}
 \pi(\{P_t\}) = & \sum_k \int \{dP_{t-2}\} \int \left[\prod_{j=1}^k dJ_j d\hat{J}_j \{d\hat{P}_j\} \right] \mathcal{P} \left[k, \{P_{t-2}\}, \mathbf{J}, \hat{\mathbf{J}}, \{\hat{\mathbf{P}}\} \right] \\
 & \times \prod_{s^t} \delta(P_t(s^t) - \phi(k, \{P_{t-2}\}, \mathbf{J}, \hat{\mathbf{J}}, \{\hat{\mathbf{P}}\}))
 \end{aligned} \tag{D.2}$$

where we have defined,

$$\begin{aligned}
 & \mathcal{P} \left[k, \{P_{t-2}\}, \mathbf{J}, \hat{\mathbf{J}}, \{\hat{\mathbf{P}}\} \right] \\
 & = \frac{1}{N} \sum_i \delta_{k,|\partial_i|} \prod_{s^{t-2}} \delta(P_{t-2}(s^{t-2}) - P_i(s^{t-2})) \\
 & \times \prod_{j \in \partial_i} \left\{ \delta(J_j - J_{ij}) \delta(\hat{J}_j - J_{ji}) \prod_{s_j^{t-1}} \delta(\hat{P}_j(s_j^{t-1}) - P_j^{(i)}(s_j^{t-1} | \hat{J}_j s^{t-2})) \right\}
 \end{aligned} \tag{D.3}$$

which is the probability that a site drawn at random has degree k , site marginal at two earlier time steps $P(s^{t-2})$, where each of the k neighbours acts on the site with interactions $\mathbf{J} = (J_1, \dots, J_k)$, and where the site acts on each neighbour with interactions $\hat{\mathbf{J}} = (\hat{J}_1, \dots, \hat{J}_k)$, and where each neighbour in the cavity graph with site i removed is described by the cavity site marginals at one earlier time step $\{\hat{\mathbf{P}}\} = (\hat{P}_1(s_1^{t-1}), \dots, \hat{P}_k(s_k^{t-1}))$. The function $\phi(k, \{P_{t-2}\}, \mathbf{J}, \hat{\mathbf{J}}, \{\hat{\mathbf{P}}\})$ is defined in equation (48). To proceed we assume that all interactions J_{ij} are drawn independently from some distribution $P(J_{ij})$, and also assume that cavity fields are independent. Under these

assumptions, we may use Bayes theorem to write,

$$\begin{aligned} \mathcal{P} \left[k, \{P_{t-2}\}, \mathbf{J}, \hat{\mathbf{J}}, \{\hat{\mathbf{P}}\} \right] \\ = P(k) \pi_{t-2} \left[\{P_{t-2}\} | k, \mathbf{J}, \hat{\mathbf{J}} \right] \prod_{j=1}^k P(J_j) P(\hat{J}_j | J_j) \hat{\pi}_{t-1} \left[\{\hat{P}_j\} | \hat{J}_j s^{t-2} \right] \end{aligned} \quad (\text{D.4})$$

where we have defined $\hat{\pi}_{t-1} \left[\{\hat{P}_j\} | x \right]$, the distribution of cavity site marginals, $\hat{P}_j(s_j^{t-1})$, given that the site removed acts on the cavity graph with external field x . We note that by definition in absence of external field the cavity distribution is equal to its non-cavity counterpart, $\hat{\pi}_{t-1} \left[\{\hat{P}_j\} | 0 \right] = \pi_{t-1} \left[\{\hat{P}_j\} \right]$, since if there is no external field, this implies that the cavity distribution is uninfluenced by the removed site, such that $\hat{J} = 0$ i.e $P_j^{(i)}(s_j^{t-1} | 0) = P_j(s_j^{t-1})$. We then insert (D.4) into (D.2) from which we find equation (47).

What remains is to find an expression for the distribution of cavity marginals $\hat{\pi}_{t-1} \left[\{\hat{P}_j\} | x \right]$. By definition this object is, in the limit $N \rightarrow \infty$, equivalent to,

$$\hat{\pi}_t \left[\{\hat{P}_i\} | x \right] = \frac{1}{N} \sum_{i\ell} \frac{A_{i\ell}}{k_i} \prod_{s_i^t} \delta \left(\hat{P}_i(s_i^t) - P_i^{(\ell)}(s_i^t | x) \right). \quad (\text{D.5})$$

We insert into (D.5) unity of the form,

$$\begin{aligned} 1 = \sum_k \delta_{k, |\partial_i|} \sum_{k'} \delta_{k', |\partial_\ell|} \int \{dP_{t-2}\} \prod_{s^{t-2}} \delta \left(P_{t-2}(s^{t-2}) - P_i(s^{t-2}) \right) \\ \times \prod_{j \in \partial_i \setminus \ell} \left\{ \int dJ_j d\hat{J}_j \delta(J_j - J_{ij}) \delta(\hat{J}_j - J_{ji}) \right. \\ \left. \times \int \{d\hat{P}_j\} \prod_{s_j^{t-1}} \delta \left(\hat{P}_j(s_j^{t-1}) - P_j^{(i)}(s_j^{t-1} | \hat{J}_j s^{t-2}) \right) \right\} \end{aligned} \quad (\text{D.6})$$

and define,

$$\begin{aligned} \mathcal{W} \left[k, k', \{P_{t-2}\}, \mathbf{J}, \hat{\mathbf{J}}, \{\hat{\mathbf{P}}\} \right] \\ = \frac{1}{N \langle k \rangle} \sum_{i\ell} A_{i\ell} \delta_{k, |\partial_i|} \delta_{k', |\partial_\ell|} \prod_{s^{t-2}} \delta \left(P_{t-2}(s^{t-2}) - P_i(s^{t-2}) \right) \\ \times \prod_{j \in \partial_i \setminus \ell} \left\{ \delta(J_j - J_{ij}) \delta(J_j - J_{ji}) \prod_{s_j^{t-1}} \delta \left(\hat{P}_j(s_j^{t-1}) - P_j^{(i)}(s_j^{t-1} | \hat{J}_j s^{t-2}) \right) \right\} \end{aligned} \quad (\text{D.7})$$

which, assuming that interactions are drawn independently, and that cavity fields are independent, can be written using Bayes theorem,

$$\begin{aligned} \mathcal{W} \left[k, k', \{P_{t-2}\}, \mathbf{J}, \hat{\mathbf{J}}, \{\hat{\mathbf{P}}\} \right] \\ = W(k, k') \pi_{t-2} \left[\{P_{t-2}\} | k, \mathbf{J}, \hat{\mathbf{J}} \right] \prod_{j=1}^{k-1} P(J_j) P(\hat{J}_j | J_j) \hat{\pi}_{t-1} \left[\{\hat{P}_j\} | \hat{J}_j s^{t-2} \right] \end{aligned} \quad (\text{D.8})$$

where $\mathcal{W} \left[k, k', \{P_{t-2}\}, \mathbf{J}, \hat{\mathbf{J}}, \{\hat{\mathbf{P}}\} \right]$ is the probability to draw a link at random connecting site i with degree k' and site j with degree k , where j has neighbours (excluding i) which act on site j with interactions $\mathbf{J} = (J_1, \dots, J_{k-1})$, and where j acts on its neighbours with interactions $\hat{\mathbf{J}} = (\hat{J}_1, \dots, \hat{J}_{k-1})$, and where the activation of each neighbour is described by the cavity site marginals $\{\hat{\mathbf{P}}\} = (\hat{P}(s_1^{t-1}), \dots, \hat{P}(s_{k-1}^{t-1}))$. We have also defined the degree correlation function $W(k, k') = (N\langle k \rangle)^{-1} \sum_{ij} A_{ij} \delta_{k', |\partial_i|} \delta_{k, |\partial_j|}$ which is the probability to draw a link at random with a node of degree k at one end and k' at the other. By writing the cavity fields as independent, we have implicitly assumed that the network lacks strong degree correlations, and so we now explicitly assume that degrees are uncorrelated such that $W(k, k') = W(k)W(k')$ where $W(k) = \frac{kP(k)}{\langle k \rangle}$ is the probability to draw a link at random that is attached to a node of degree k . Substituting this form of unity into the definition for the cavity marginal (D.5) we find equation (49). Equations (47) and (49) are a closed set of equations which may be solved via a population dynamics procedure. Note, this a dynamical variant of the population dynamics procedure, and can be used to compute the distribution of site marginals at each point in time.

From the distributional equations (47) and (49), one can also derive a closed set of equations for the *average* site marginal, which by definition is given by,

$$\bar{P}_t(s^t) = \int \{dP_t\} \pi(\{P_t\}) \{P_t\}. \quad (\text{D.9})$$

If we substitute equation (47) into (D.9) we find,

$$\begin{aligned} \bar{P}_t(s^t) &= \sum_k P(k) \int \left[\prod_{j=1}^k dJ_j d\hat{J}_j \{d\hat{P}_j\} P(J_j) P(\hat{J}_j | J_j) \right] \\ &\times \sum_{s^{t-2}} \bar{P}_{t-2}(s^{t-2} | k, \mathbf{J}, \hat{\mathbf{J}}) \sum_{s_1^{t-1}, \dots, s_k^{t-1}} W(s^t | \sum_{j=1}^k J_j s_j^{t-1}) \\ &\times \prod_{j=1}^k \left[(1 - \delta_{J_j, 0}) \bar{Q}_{t-1}(s_j^{t-1} | \hat{J}_j s_j^{t-2}) + \delta_{J_j, 0} \bar{P}_{t-1}(s_j^{t-1}) \right] \end{aligned} \quad (\text{D.10})$$

where we have defined,

$$\bar{Q}_t(s^t | x) = \int \{d\hat{P}\} \hat{\pi}(\{\hat{P}_t\} | x) \{P_t\}. \quad (\text{D.11})$$

If we then insert equation (49) into (D.11), we find,

$$\begin{aligned} \bar{Q}_t(s^t|x) &= \sum_k \frac{kP(k)}{\langle k \rangle} \int \left[\prod_{j=1}^{k-1} dJ_j d\hat{J}_j \{d\hat{P}_j\} P(J_j) P(\hat{J}_j|J_j) \right] \\ &\times \sum_{s^{t-2}} \bar{P}_{t-2}(s^{t-2}|k, \mathbf{J}, \hat{\mathbf{J}}) \sum_{s_1^{t-1}, \dots, s_{k-1}^{t-1}} W(s^t | \sum_{j=1}^{k-1} J_j s_j^{t-1} + x) \\ &\times \prod_{j=1}^{k-1} \left[(1 - \delta_{j,0}) \bar{Q}_{t-1}(s_j^{t-1} | \hat{J}_j s_j^{t-2}) + \delta_{j,0} \bar{P}_{t-1}(s_j^{t-1}) \right]. \end{aligned} \quad (\text{D.12})$$

Equations (D.10) and (D.12) are a closed set of equations that may be solved via iteration. These equations may also be derived via generating functional analysis, if one makes appropriate assumptions to deal with memory effects [40].

References

- [1] Hatchett J P and Kühn R 2009 *Quantitative Finance* **9** 373–382
- [2] Gu J W, Ching W K, Siu T K and Zheng H 2013 *Risk and Decision Analysis* **4** 119–129
- [3] Liang R, Qiu Y and Ching W K 2014 Construction of probabilistic boolean network for credit default data 2014 *Seventh International Joint Conference on Computational Sciences and Optimization* (IEEE) pp 11–15
- [4] Zhu P, Song X, Liu L, Wang Z and Han J 2018 *IEEE access* **6** 35292–35304
- [5] Green D G, Leishman T G and Sadedin S 2007 The emergence of social consensus in boolean networks 2007 *IEEE Symposium on Artificial Life* (IEEE) pp 402–408
- [6] Li B, Wu J, Qi H, Proutiere A and Shi G 2017 *IEEE/ACM Transactions on Networking* **26** 118–130
- [7] Kauffman S A 1969 *Journal of theoretical biology* **22** 437–467
- [8] Kauffman S 1969 *Nature* **224** 177–178
- [9] Liang J and Han J 2012 *BMC systems biology* **6** 1–21
- [10] Hannam R, Kuehn R and Annibale A 2019 *Journal of Physics A: Mathematical and Theoretical* **52** 334002
- [11] Torrisi G, Kühn R and Annibale A 2020 *Journal of Statistical Mechanics: Theory and Experiment* **2020** 083501
- [12] Torrisi G, Kühn R and Annibale A 2022 *arXiv preprint arXiv:2202.06705*
- [13] Folli V, Gosti G, Leonetti M and Ruocco G 2018 *Neural Networks* **104** 50–59
- [14] Neri I and Bollé D 2009 *Journal of Statistical Mechanics: Theory and Experiment* **2009** P08009
- [15] Aurell E and Mahmoudi H 2011 *Journal of Statistical Mechanics: Theory and Experiment* **2011** P04014
- [16] Aurell E and Mahmoudi H 2012 *Physical Review E* **85** 031119
- [17] Zhang P 2012 *Journal of Statistical Physics* **148** 502–512
- [18] Torrisi G, Annibale A and Kühn R 2021 *Physical Review E* **104** 045313
- [19] Mozeika A and Saad D 2012 *Philosophical Magazine* **92** 210–229
- [20] Peretto P 1984 *Biological cybernetics* **50** 51–62
- [21] Skantzos N and Coolen A 2000 *Journal of Physics A: Mathematical and General* **33** 1841
- [22] Skantzos N and Coolen A 2001 Random field ising chain and neutral networks with synchronous dynamics *AIP Conference Proceedings* vol 553 (American Institute of Physics) pp 101–106
- [23] Fontanari J and Köberle R 1988 *Journal de Physique* **49** 13–23

- [24] Castillo I P and Skantzos N 2004 *Journal of Physics A: Mathematical and General* **37** 9087
- [25] Mézard M and Parisi G 2001 *The European Physical Journal B-Condensed Matter and Complex Systems* **20** 217–233
- [26] Parisi G, Ricci-Tersenghi F and Rizzo T 2014 *Journal of Statistical Mechanics: Theory and Experiment* **2014** P04013
- [27] Altieri A, Angelini M C, Lucibello C, Parisi G, Ricci-Tersenghi F and Rizzo T 2017 *Journal of Statistical Mechanics: Theory and Experiment* **2017** 113303
- [28] Thouless D 1986 *Physical review letters* **56** 1082
- [29] Carlson J, Chayes J, Chayes L, Sethna J and Thouless D 1990 *Journal of statistical physics* **61** 987–1067
- [30] Carlson J, Chayes J, Sethna J P and Thouless D 1990 *Journal of statistical physics* **61** 1069–1084
- [31] Sompolinsky H, Crisanti A and Sommers H J 1988 *Physical review letters* **61** 259
- [32] Rieger H, Schreckenberg M and Zittartz J 1989 *Zeitschrift für Physik B Condensed Matter* **74** 527–538
- [33] Ma Y Q, Zhang Y M and Gong C D 1992 *Communications in Theoretical Physics* **18** 491
- [34] Franz S, Leone M, Ricci-Tersenghi F and Zecchina R 2001 *Physical Review Letters* **87** 127209
- [35] Ricci-Tersenghi F, Weigt M and Zecchina R 2001 *Physical Review E* **63** 026702
- [36] Mézard M, Ricci-Tersenghi F and Zecchina R 2002 *Jour. of Statistical Physics* **111** 105
- [37] Hatchett J, Wemmenhove B, Castillo I P, Nikolettopoulos T, Skantzos N and Coolen A 2004 *Journal of Physics A: Mathematical and General* **37** 6201
- [38] Mimura K and Coolen A 2009 *Journal of Physics A: Mathematical and Theoretical* **42** 415001
- [39] Hurry C J, Mozeika A and Annibale A 2022 *Journal of Statistical Mechanics: Theory and Experiment* **2022** 033302
- [40] Hurry C J 2022 *Statistical mechanics of immunity from genes to populations* Ph.D. thesis King's College London